Available online at www.sciencedirect.com
SCIENCE DIRECT
ELSEVIER
Coordination Chemistry Reviews 249 (2005) 2740–2762
COORDINATION CHEMISTRY REVIEWS
www.elsevier.com/locate/ccr

Review

DFT study of "all-metal" aromatic compounds

Constantinos A. Tsipis *

Laboratory of Applied Quantum Chemistry, Department of General and Inorganic Chemistry, Faculty of Chemistry, Aristotle University of Thessaloniki, 541 24 Thessaloniki, Greece

Accepted 28 January 2005
Available online 22 March 2005

Contents

1. Introduction 2740
2. Aromaticity: the most vexing and fascinating key chemical concept 2741
3. "Types" of aromaticity 2741
4. "Diagnosis" of aromaticity 2743
   4.1. Energetic criteria of aromaticity 2743
   4.2. Structural or geometric criteria of aromaticity 2744
   4.3. Magnetic criteria of aromaticity 2744
   4.4. Chemical reactivity criteria of aromaticity 2745
   4.5. Electronic criteria of aromaticity 2745
5. *cyclo*-Gallenes and metallaromaticity 2746
6. Aromatic metal clusters 2747
   6.1. All-metal aromatic molecules 2747
   6.2. Ligand-stabilized all-metal $[M_nL_m]$ aromatic molecules 2755
   6.3. Hydrometal analogues of aromatic hydrocarbons 2758
7. Conclusions and perspectives 2759
   References 2759

Abstract

An overview of recent quantum chemical studies on all-metal aromatic compounds is presented. Novel classes of inorganic molecules containing bonds that are characterized by a common ring-shaped electron density are reviewed. The mechanistic insight gained for the aromatic character of all-metal aromatic molecules is discussed and the predictive nature of the electronic structure calculation methods particularly those based on density functional theory (DFT) is highlighted. The indicators of aromaticity (aromaticity criteria) – structural, magnetic, energetic and reactivity-based measures – many of which are accessible through quantum chemical calculations are also outlined herein.

Keywords: All-metal aromatic compounds; Aromaticity; DFT; Aromatic metal clusters; Aromatic criteria

1. Introduction

This review is based on the following premises: (i) that computational chemistry is a key to the understanding and predicting the behavior of a broad range of chemical, physical, and biological phenomena and to our efforts to change the scientific landscape in the 21st century, (ii) that chemical structure encoding the physical, chemical, biological, and technical properties of molecules provides means to routinely design novel classes of chemical compounds, catalysts and other materials and predict biological activity or

* Tel.: +30 2310 997851; fax: +30 2310 997851.
E-mail address: tsipis@chem.auth.gr.

0010-8545/$ – see front matter © 2005 Elsevier B.V. All rights reserved.
doi:10.1016/j.ccr.2005.01.031

environmental fate; and (iii) that the aromaticity concept – the cornerstone for rationalizing and understanding the structure and thus the behavior of the so-called aromatic organic compounds – is also applicable within the realm of inorganic chemistry for a number of all-metal molecules and other coordination and organometallic compounds.

2. Aromaticity: the most vexing and fascinating key chemical concept

Let us first pay tribute to the elusive character of the concept of aromaticity. Aromaticity has almost exclusively fallen within the realm of organic chemistry, benzene being the quintessential example. From an inorganic perspective, the concept of aromaticity has been the unique domain of borazine – the boron–nitrogen six-membered ring compound often referred to as "inorganic benzene". Aromaticity is one of the most general but at the same time one of the most vaguely defined chemical concept. Even though this concept was introduced in 1865–1866 by Kekulé [1–7] it has no precise and generally well established definition yet. As a consequence of the lack of a universally acceptable/applicable definition of aromaticity, the term is understandably controversial. We are not wishing to indulge ourselves in joining the ongoing passionate discussion on this subject, we merely note that despite the frequent use of the term "aromaticity" in the past and present literature, aromaticity is not a measurable quantity and must be defined by convention. Although the term "aromaticity" remains somewhat nebulous, it is generally agreed that aromatic compounds exhibit special characteristics that distinguish them from nonaromatic compounds. At the very beginning *aromaticity was considered as the property of planar conjugated cyclic π-electron compounds that exhibit cyclic π-electron delocalization* (*CED*) *in their ground state* manifested by the following set of distinguishing molecular features:

- An *extra stabilization* with respect to their noncyclic analogues. In this context aromaticity is defined as the difference between π-electron resonance energies of a noncyclic π-conjugated compound and a cyclic π-conjugated compound, giving rise to the venerable Hückel's $(4n + 2)\pi$-electron-counting rule of aromaticity [8].
- A *bond length equalization*: The bonds constituting the aromatic ring acquire a partial double bond character.
- A *specific response to externally applied uniform magnetic field* perpendicular to the molecular plane. This response is associated with the ability of the ring to sustain an induced diamagnetic (diatropic) ring current.
- A *tendency to undergo electrophilic substitution* rather than *addition* reactions.
- A *strong usually pleasant odor, an* "*aroma*" from the ancient Greek word άρωμα exhibited by the archetypal aromatic system, the benzene molecule.

Timely exhaustive assessments of the aromaticity concept have been covered in several of the articles in a thematic issue of *Chemical* Reviews [9–18] and a very recent special issue of *Physical Chemistry Chemical Physics* [19–34]. Moreover, an excellent publication by Minkin et al. [35] in 1994 entitled *Aromaticity and Antiaromaticity: Electronic and Structural Aspects*, and a more recent work by Katritzky and co-workers [36] offer an excellent discussion of the problems associated with defining aromaticity.

3. "Types" of aromaticity

The field of aromaticity continues to be controversial. The central theme of this controversy is the definition of aromaticity itself. Today, the proliferation of "types" of aromaticity goes far beyond the conventional confines and has been extended to include heterosystems [37,38], chelate metallacycles in which metalloaromaticity stabilizes coordinated chelate ligands [39], inorganic molecules [40,41], and transition metal oxides [42]. A considerable number of prefixes joined to the term of aromaticity (*anti-*, *non-*, *homo-*, *quasi-*, *pseudo-*, etc.) and other "types" of aromaticity suggested so far, such as classical aromaticity, magnetic aromaticity, Möbius aromaticity, σ-aromaticity, local-aromaticity, 3D-aromaticity and spherical aromaticity pose additional problems. All these terms related to specific properties of the molecular system illustrate that aromaticity should take into consideration multiple structural, chemical and physical manifestations – it must be a multi-dimensional phenomenon. In the following we will briefly outline the various "types" of aromaticity for the reader to get insight into the complexity of the vexing and nebulous concept of aromaticity:

1. *Antiaromaticity* is the property of a closed-shell cyclic planar conjugated π-electron system having $4n$ instead of $(4n + 2)\pi$ electrons. A representative example is the cyclobutadiene molecule. The antiaromaticity may be reduced when the molecule may become nonplanar (such as cyclooctatetraene). An excellent account of the antiaromaticity in monocyclic conjugated carbon rings by Wiberg [26] is enthusiastically commended to the readers of this present issue of *Coordination Chemistry Reviews*.
2. *Homoaromaticity* is the property of compounds that display aromaticity despite one or more saturated linkages interrupting the formal cyclic conjugation [43]. A representative example is the tris-homocyclopropenyl cation, **1**.

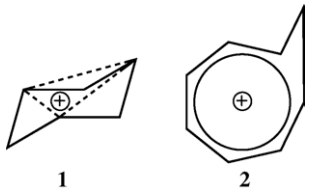

1 **2**

Homoaromaticity is well-established in cationic and anionic systems where delocalization of charge provides an additional driving force for homoaromaticity. Neutral radicals do not participate in homoconjugation and are not expected to exhibit homoaromaticity. A family of potentially homoaromatic molecules can be derived from cyclic and conjugated $(4n+2)\pi$-electron hydrocarbon species by inserting a CH_2 unit into the molecular ring. The best-known example of this kind of species is probably the homotropylium, **2**. A recent scholarly and authoritative survey of homoaromaticity by Williams [21] is very informative.

3. *Quasi-aromaticity* is the property of transition metal cluster compounds with the general formula $[M_3(\mu_3\text{-}X)(\mu\text{-}Y)_3]^{4+}$ containing a puckered $[M_3(\mu\text{-}Y)_3]$ six-membered ring, which exhibits benzene-like structural characteristics and chemical behavior in a series of ligand substitution, addition and redox reactions [44–46]. The energy-localized molecular orbital (LMO) analysis indicated that the *quasi*-aromaticity in these puckered $[M_3X_3]$ six-membered ring clusters is related to a set of three continuous and closed 3c–2e (d-p-d)π bonds with strong interactions, which account for their stability, reactivity and spectroscopy. The orbital interactions describing the 3c–2e (d-p-d)π bonds in $[M_3X_4]$ (X_c is a triply-bridged or capping atom and X_b are edge-bridging atoms) cluster core are depicted schematically in **3**.

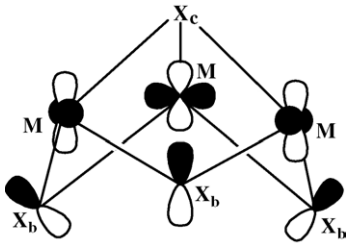

3

4. *Classical aromaticity* is an aromaticity scale based on the geometric and energetic criteria of aromaticity. It was introduced in a series of papers entitled "*Aromaticity as a Quantitative Concept*" by Katritzky et al. [47–50] as a result of the principal component analysis (PCA) of 12 common quantitative criteria of aromaticity.
5. *Magnetic aromaticity* is an aromaticity scale based on the magnetic criteria of aromaticity. It is the second component of the PCA analysis, which is orthogonal to the classical one.
6. *Möbius aromaticity* is the property of compounds with rigid frameworks that enforce a smoothly twisted conjugation. In Möbius aromaticity a monocyclic array of orbitals in which there is a single or generally an odd number of out-of-plane overlaps reveals the opposite pattern of aromatic character to Hückel systems; with $4n$ π electrons it is stabilized (aromatic), whereas with $(4n+2)\pi$ electrons it is destabilized (antiaromatic). The concept of Möbius aromaticity was first introduced by Heilbronner [51], with its name derived from the topological analogy of such an arrangement of orbitals to a Möbius strip. A Möbius structure can be considered as a combination of a "normal" aromatic structure and a belt-shaped aromatic structure as depicted graphically in Scheme 1 [52].
7. *σ-Aromaticity* is the aromaticity due to the cyclic σ-electron delocalization first developed by Dewar [53–56] and later Exner and Schleyer [57] to account for the stability and properties of cyclopropane derivatives. A review by Cremer [58] provides an informative summary of the key concept of σ-aromaticity. A more recent example of σ-aromaticity concerns the bonding in triangular metal carbonyl clusters reported by King [59]. The σ-aromatic model for $M_3(CO)_{12}$ (M = Fe, Ru, Os), **4**, involves the 3c–2e core bond with Hückel topology and the 3c–4e perimeter bond with Möbius topology, **5**.

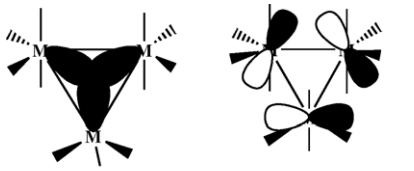

5

8. *Local aromaticity* is the aromaticity of an individual benzene ring in polycyclic systems. Dewar explicitly mentioned extending the notion of aromaticity criteria to individual rings in polycyclic systems [60]. Polansky and Derflinger [61] derived a ring index as a measure of the "benzene character" of individual benzene rings in polycyclic benzenoid hydrocarbons. This ring index is determined from computed MO coefficients when the MO's of the system are expanded in sets of MO's of each ring. In other words, the "benzene character" "*is the projection of occupied π-MO's in a given hexagon L of a polycyclic benzenoid hydrocarbon onto the three occupied MO's of a benzene molecule located on that position*" [62].
9. *3D-aromaticity* is the aromaticity of three-dimensional delocalized systems with near spherical geometries, such as deltahedral boranes and carboranes, hydrogen and lithium clusters, Zintl ions and fullerenes. It was found that the highest degree of aromaticity could only be achieved in systems with fully occupied valence shells. It should be noted that the 3D-aromaticity is guided by the $2(N+1)^2$ counterpart of the Hückel rule. A review by King [42] on the three-dimensional aromaticity in diverse deltahedral boron based clusters and related molecules is very informative.
10. *Spherical aromaticity* is synonym with 3D-aromaticity. It is the aromaticity exhibited by icosahedral fullerenes which are spherical molecules containing a conjugated π-electron system. Again icosahedral fullerenes that contain $2(N+1)^2\pi$ electrons show the maximum

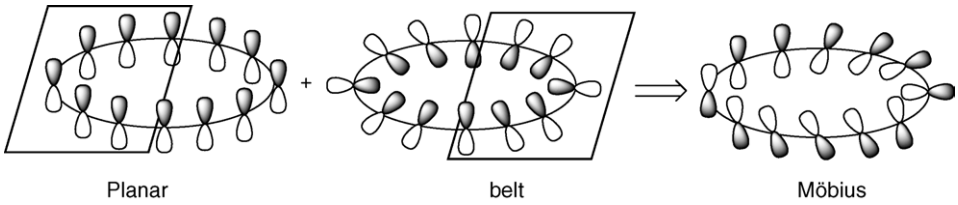

Scheme 1. Schematic construction of a Möbius structure. Reproduced with permission from [52]. Copyright by Wiley-VCH Verlag GmbH&Co. KgaA, Weinheim.

degree of spherical aromaticity. This is closely related to the stable noble-gas configuration of atoms or atomic ions. The nature of fullerene aromaticity considering count rules involving the whole π-electron system and the relationship between the buildup of electrons in atomic π-electron shells and the spherical aromaticity of icosahedral fullerenes has been recently surveyed by Bühl and Hirsch [20]. Recently [63], the $2(N+1)^2\pi$-electron-counting rule was applied in a family of three-dimensional homoaromatic systems, such as cubane, dodecahedrane, and adamantine frameworks, thus introducing one more "type" of aromaticity that of *spherical homoaromaticity*. Reiher and Hirsch [64] studied spherical aromaticity from the point of view of atomic structure theory introducing the "pseudo-atom" model of spherical clusters and fullerenes. According to this model, the characteristic features of polyhedral molecules and fullerenes that obey the $2(N+1)^2$ rule of spherical aromaticity can be related to energetically stable ground-state closed-shell configurations of (pseudo-)atoms. The "pseudo-atom" model of spherical aromaticity explains and justifies the pseudo-*l* classification of molecular orbitals, which is the basis of the $2(N+1)^2$ rule, and provides a unified view on the stability of rare gas atoms and aromatic spherical polyhedra. The "pseudo-atom" model of spherical clusters and fullerenes has some similarities with the so-called "jellium" model in physics for description of the shape and stability of metal clusters [65–67]. The "jellium" model offers a simple explanation for the observed electron counts (the magic numbers 2, 8, 20, 32, 40, 50, . . .) of spherical metal clusters with particular stability. However, since the "jellium-type" model studies have not established any relation between the stability of different hollow cluster structures and their aromaticity, a more detailed discussion of the "jellium-type" models is out of the scope of this review.

4. "Diagnosis" of aromaticity

Because of the importance of aromaticity in chemistry, there have been many attempts to rationalize and quantify this property, and to derive a universal quantitative measure of it. However, because of its multiple manifestations, there is not yet any generally accepted single quantitative definition of aromaticity. The evaluation of aromaticity is usually based on the classical aromaticity criteria, which can roughly be divided into four categories: energetic, structural or geometrical, magnetic, and reactivity-based measures [29,36]. One can also add a fifth category based on electronic measures derived by the powerful electronic structure calculation tools (ab initio and DFT) [9,18,33,68]. The literature on aromaticity and its measures is so vast that I must be content here with outlining briefly the aromaticity criteria and making comprehensive reference only to a selection of the more recent reviews and articles in the field.

4.1. Energetic criteria of aromaticity

The energetic criteria of aromaticity make use of the fact that conjugated π-electron compounds are more stable than their chain analogs. When using the energetic criterion of aromaticity, one compares the excess of stability of the structure due to cyclic electron delocalization relative to a well-chosen reference system, in most cases olefins or conjugated polyenes [34–36,69]. The most commonly used measure among energetic criteria of aromaticity is the aromatic stabilization energy (ASE), calculated as the energetic effect of an imaginary homodesmotic reaction [70–72]. A representative example of a homodesmotic reaction is that referred to benzene molecule:

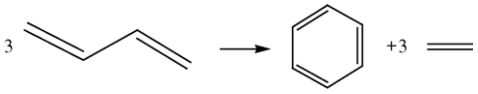

In a homodesmotic reaction there must be equal numbers of atoms in their various states of hybridization in both the reactants and products and also there must be a matching of element–hydrogen bonds in terms of the number of hydrogen atoms joined to the individual elements in the reactants and products.

Energetic data can be gathered from experiment and from quantum chemical calculations. The ASE depends dramatically on the kind of reaction and the level of the theory applied. Therefore, it is important to use accurate energetic data (from high quality quantum chemical computational methods) and to use a well-chosen "reference" structure. The choice of an appropriate reference system in the calculation of the resonance energy can be avoided when applying the so-called spin-coupled theory, developed by Cooper et al. [73–75]. Moreover, perturbing influences, such as strain and the presence of heteroatoms, complicating the evaluation of

aromatic stabilization energies are overcome easily by employing the "isomerization method" suggested by Schleyer and Puhlhofer [76]. This is based on the differences (ISE) between total energies computed for only two species: a methyl derivative of the aromatic system and its nonaromatic exocyclic methylene isomer.

4.2. Structural or geometric criteria of aromaticity

The structural or geometric criteria of aromaticity are based on the important manifestations of aromaticity those of the bond length equalization, planarity and symmetry. On the basis of geometrical considerations, molecules should show a decrease in aromatic character when they possess a high degree of bond alternation and deviate significantly from planarity. Several quantitative measures of this bond alternation have been proposed [28]. Among the most important geometric indices of aromaticity, one of the most effective is the harmonic oscillator model of aromaticity (HOMA) defined by Kruszewski and Krygowski [77,78] according to the equation:

$$\mathrm{HOMA} = 1 - \frac{\alpha}{n}\sum(R_{\mathrm{opt}} - R_{\mathrm{i}})^2$$

where n is the number of bonds taken into the summation and α is an empirical constant chosen to give HOMA = 0 for the hypothetical Kekulé structures of the aromatic systems and 1 for the system with all bonds equal to the optimal value R_{opt}. The quantity R_{opt} is defined as a length of the CC bond for which the energy (estimated by use of the harmonic potential) of the compression to the length of a double bond and expansion to the length of a single bond in 1,3-butadiene is minimal. The quantity R_{i} stands for the individual bond lengths. To apply the HOMA index to study the aromatic character of a given π-electron system the following data are needed: (i) the precise geometry of the studied molecule, i.e., its bond lengths R_{i}, (ii) the optimized values R_{opt} for all relevant bonds and (iii) the values for the relevant constants α.

4.3. Magnetic criteria of aromaticity

The magnetic criteria of aromaticity are based on the specific response of the aromatic compounds to externally applied uniform magnetic field perpendicular to the molecular plane. Several magnetic criteria have been put forward as measurements of the aromaticity of molecules [11,14,17,27–29,33]. Magnetic aromaticity can be defined as the ability of a compound to sustain an induced ring current; these compounds are then called *diatropic*. Antiaromatic compounds are called *paratropic*. Several methods can be used to measure if a compound can sustain a ring current. Historically, characteristic proton NMR chemical shifts and the exaltation of magnetic susceptibility (Λ) have been important magnetic criteria for quantification of aromaticity. Protons attached to aromatic rings typically undergo a downfield shift from the olefinic region. However, when the protons are above or in the aromatic ring, as, e.g., in the case of the inner protons of [n] annulenes, an upfield shift is noticed in the ^{1}H NMR spectrum. For antiaromatic compounds, these directions are the opposite. Mitchell has recently proposed measuring aromaticity by NMR spectroscopy [30]. Concerning the diamagnetic susceptibilities, two factors are important when measuring a compound's aromaticity: the anisotropy [79,80] and the exaltation [81]. Aromatic molecules were found to possess high diamagnetic susceptibility anisotropies $\Delta\chi^{\mathrm{m}}$, defined as:

$$\Delta\chi^{\mathrm{m}} = \chi^{\mathrm{m}}_{zz} - \frac{1}{2}\{\chi^{\mathrm{m}}_{xx} + \chi^{\mathrm{m}}_{yy}\}$$

where χ^{m}_{zz}, χ^{m}_{xx}, and χ^{m}_{yy} are the three principal components of the diamagnetic susceptibility.

The magnetic exaltation is defined as the difference between the true mean molar magnetic susceptibility $\overline{\chi}^{\mathrm{m}}$ and the one calculated by a hypothetical, additive incremental scheme by use of atom and bond increments $\chi^{\mathrm{m}}_{\mathrm{cacl}}$, according to the equation:

$$\Lambda^{\mathrm{m}} = \overline{\chi}^{\mathrm{m}} - \chi^{\mathrm{m}}_{\mathrm{calc}}$$

The exaltations are negative (diamagnetic) for aromatic compounds and positive (paramagnetic) for antiaromatic compounds.

Ring-current intensities have also been used as a criterion for aromaticity [27,82]. In their outstanding article in the recent *Chemical Reviews* issue on aromaticity, Gomes and Mallion [27] reported on aromaticity as viewed from the model of ring currents. Modeling magnetic properties and chemical shifts of benzenoid compounds on the ring-current idea is a very natural "miniature" of the ideas of the classical physics described by Kirchhoff's laws. Haigh and Mallion [83] established a theoretical basis for relating the incidence of relatively "high" and "low" ring-current intensities to the intuitive VB resonance theory and the "bond fixation" in conjugated compounds. An authoritative, definitive and highly readable account by Lazzeretti [82] entitled *Ring Currents* published in a recent issue of *Progress in Nuclear Magnetic Resonance Spectroscopy* is very informative and is highly commended.

It has long been recognized that the conjugated system of π electrons in an aromatic compound supports a ring current, which exerts a deshielding effect on atoms outside the ring and a shielding effect on atoms inside the ring. The shielding tensor $\vec{\vec{\sigma}}$ describes the relation between applied (external $\vec{B}_{\mathrm{ext}}$) and induced magnetic field ($\vec{B}_{\mathrm{ind}}$):

$$\vec{B}_{\mathrm{ind}}(\vec{R}) = -\vec{\vec{\sigma}}(\vec{R})\vec{B}_{\mathrm{ext}}$$

The induced magnetic field at position $\vec{R}$ can be computed from the current density $\vec{j}(\vec{r})$ applying Biot-Savart's law:

$$\vec{B}_{\mathrm{ind}}(\vec{R}) = \frac{\mu_0}{4\pi}\int \frac{\vec{j}(\vec{r}) \times (\vec{r} - \vec{R})}{|\vec{r} - \vec{R}|^3}\,\mathrm{d}^3r$$

The shielding tensor can be computed from the current density, which itself is induced by the external magnetic field $\vec{B}_{\mathrm{ext}}$.

The current density is a 3D vector-field defined at any point in space. The topological analysis of the current fields has been used as a means of describing the calculated current fields, which are difficult to visualize in their full detail and complexity. The current density at a given point in space can be evaluated assuming that the same point lies at the origin of the coordinate system. To this end the CTOCD-DZ (continuous transformation of origin of the current density-diamagnetic zero) formulation of magnetic response, the so-called *ipsocentric* method [84–89] provides current density maps of high quality. Moreover, for an N-electron system, the total current density may be broken down into additive orbital components. Steiner and Fowler in a series of papers [90–92] showed that orbital decomposition lends itself to rationalization of the link between magnetic aromaticity and electron-count in conjugated π systems. The ipsocentric distribution of origin of vector potential is the only distribution that gives rise to a clear physical separability of orbital contributions. The very recent outstanding article on the orbital analysis of magnetic properties by Steiner and Fowler [13] is also very informative. Finally, the response of a molecule to an applied external magnetic field can be evaluated by a graphical representation of the induced magnetic field [93]. It was shown that molecules that contain a π-electron system possess a long-range magnetic response, while the induced magnetic field is short–range for molecules without π-electron system.

More recently, a new and widely used index of aromaticity, the nucleus-independent chemical shift (NICS), has been proposed by Schleyer et al. [69,94]. It is defined as the negative value of the absolute shielding computed at a ring center or at some other interesting points of the system. Negative NICS values correspond to aromaticity (e.g., −11.5 ppm for benzene), while positive values are associated with antiaromaticity (e.g., +28.8 ppm for cyclobutadiene). The more negative the NICS values, the more aromatic are the rings. There is a whole family of NICS methods, which include NICS computations at ring centers [94], NICS(0) and above [95], NICS(1) and NICS(2), dissected NICS values, i.e., the total NICS at a particular point in space may be dissected into paratropic and diatropic components, which mainly arise from the C–C σ and π multiple bonds, respectively [95,96], and MO contributions to NICS, MO–NICS, $NICS_\pi$ [14,97]. NICS may be mapped in three-dimensional space [98,99]; significantly negative NICS values along the direction normal to a ring system indicate the presence of induced diatropic ring currents, a characteristic of cyclic electron delocalization.

4.4. Chemical reactivity criteria of aromaticity

The chemical reactivity criteria of aromaticity are based on the chemical behavior, i.e., the reactivity of the system. Aromatic compounds will in most cases tend to react in such a fashion as to retain their π-electron system and will thus prefer to undergo electrophilic substitution instead of addition reactions. Not many indices have tried to quantify this effect in order to probe the aromaticity, and exceptions to the rule that aromatic compounds undergo electrophilic substitution rather than addition reactions are known [100,101]. The problem with the reactivity criterion of aromaticity is that it depends on the difference of the free energy of the ground state of the molecule and the transition state of the reaction. In this sense it is not easy to quantify, because it does not depend on the ground state alone and may vary with the choice of the reagent.

4.5. Electronic criteria of aromaticity

The electronic criteria of aromaticity are based on the electron density $\rho(\mathbf{r})$ of the aromatic system. The topology of the electron density has been used to quantify the aromaticity of molecules. The use of electronic criteria of aromaticity is less common. Among them, we will mention the HOMO–LUMO energy gap, the absolute and relative hardness, the electrostatic potential, the polarizability, the electron localization function (ELF) analysis of the electron density, and the delocalization index (DI) of aromaticity [33,68,102]. Natural bond orbital (NBO) analysis of the first-order density has also been used to quantify aromaticity [103,104]. In addition, an aromaticity index that takes account of the topological properties of the electron density at ring-critical points of six-membered rings using the Bader's Atoms in Molecules (AIM) theory [105–107] has been also proposed [108]. We direct interested readers to the article by De Proft and Geerlings [33] and the references cited therein for more information on some of the electronic criteria of aromaticity introduced by conceptual DFT.

The global hardness η defined as the difference between the eigenvalues of the LUMO and HOMO:

$$\eta = \varepsilon_{\mathrm{LUMO}} - \varepsilon_{\mathrm{HOMO}}$$

is a measure of the stability via the maximum hardness principle formulated by Pearson [109]. It is obvious then, that a well-defined "relative hardness" $\Delta\eta$, that is the difference between the hardness of the π-electron conjugated system and that of a "reference" chosen according to the isomerization method should be a good measure of aromaticity.

The molecular electrostatic potential topography has also proposed as a measure of aromaticity in a series of polycyclic benzenoid hydrocarbons by Suresh and Gadre [110]. The electron localization function (ELF) defined as:

$$\mathrm{ELF} = \frac{1}{1 + (D/D_\mathrm{h})^2}$$

where

$$D = \frac{1}{2}\sum_i |\nabla\psi_i(\mathbf{r})|^2 - \frac{1}{8}\frac{|\nabla\rho(\mathbf{r})|^2}{\rho(\mathbf{r})}$$

and

$$D_\mathrm{h} = \frac{3}{10}(3\pi^2)^{2/3}\rho(\mathbf{r})^{5/3}$$

was found to be a good measure of aromaticity in a series of substituted five-membered cyclopentadienyl systems [111]. The topological analysis of the ELF provides a picture in which the electron density is distributed and localized in different volumes called basins, thus enabling one to discuss the reliability of simplified representations of electron densities in terms of superposition of promolecular densities or resonant Lewis structures. Finally, the delocalization index δ(A, B) derived from the AIM theory was proposed as another possible electronic index of aromaticity [68,112–117].

Finally, Sakai [118,119] presented a new electronic criterion of aromaticity for benzene-like molecules with six-membered rings on the basis of a CiLC method in reference to ab initio molecular orbital (MO) calculations. The CiLC method is a combination of configuration interaction (CI), localized molecular orbital (LMO), and complete active space self-consistent field (CASSCF) analysis. The new criterion of aromaticity for six-membered rings, such as C_6H_6, Si_6H_6, B_6, Al_6, N_6, and P_6, was defined, taken as the degree of equality of electronic structures for each of the bonds in the six-membered ring and by the narrowness of the gap between the weights of the singlet coupling and polarization terms for each bond. The new criterion was extended to cyclic C_nH_n (n = 4, 6, 8, and 10) compounds, where another index of aromaticity for ring-unit compounds – the index of deviation from aromaticity (IDA) – was also proposed [120].

Summarizing the diagnostics of aromaticity it should be stressed that the concept of aromaticity must be analyzed in terms of a multiplicity of measures, since no single property exists whose measurement could be taken as a direct, unequivocal measure of aromaticity. This is especially true for the indicators, which are calculated from the differences of the properties of the parent and a reference system. However, as far as the "all-metal" aromatic systems are concerned, the use of both the magnetic and electronic criteria of aromaticity is recommended.

5. *cyclo*-Gallenes and metallaromaticity

The first example of an aromatic metallic system, namely *cyclo*-gallene dianion, formulated as $[cyclo\text{-}Ga_3L_3]^{2-}$ (L = $Mes_2C_6H_3$, 2,6-dimesitylphenyl), **6**, has been reported in the middle of 90s [121]. The *cyclo*-gallene dianion exhibits a perfectly planar geometry of high symmetry with Ga–Ga bond distances of 244.1 pm (among the shortest ones) and Ga–Ga–Ga bond angles of 60.0° The aromatic character of **6** was assessed by calculating the absolute magnetic shieldings at selected points in space as a function of the electron density [122]. Upfield changes of the chemical shifts for the alkali metal counterions over and under the ring plane by 6, 57 and 108 ppm for Li, Na and K, respectively, are indicative of induced ring currents in the Ga_3 metallic ring, a magnetic criterion for aromaticity. The aromatic character of the Ga_3 metallic ring was further substantiated by the large negative NICS(0) values ranging from −13.0 to −17.6 ppm. The $[cyclo\text{-}Ga_3L_3]^{2-}$, being a 2π-electron aromatic system, bears a striking electronic resemblance to the well-known 2π-electron triphenylcyclopropenium cation, **7** [123]. Electronic structure calculations at the HF and B3LYP levels of theory on the $[cyclo\text{-}Ga_3]^{2-}$ anionic core, in $[cyclo\text{-}Ga_3H_3]^{2-}$, **8**, $Na_2[cyclo\text{-}Ga_3H_3]$ and $K_2[cyclo\text{-}Ga_3H_3]$ suggested a well-defined π-molecular orbital. The cyclic 2π-electron density delocalization in **8** closely resembles that of a $4n + 2$ (n = 0) Hückel aromatic system [124]. Both experimental and theoretical results strongly supported the *cyclo*-gallene dianion $[(Mes_2C_6H_3)_3Ga_3]^{2-}$, as a well-defined metalloaromatic system – a metallic ring system exhibiting aromaticity.

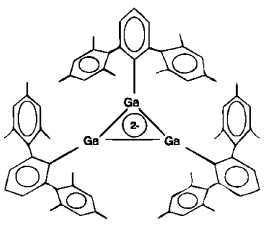

6

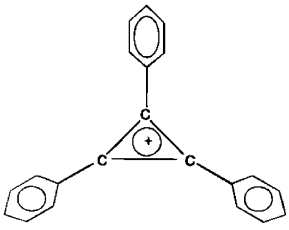

7

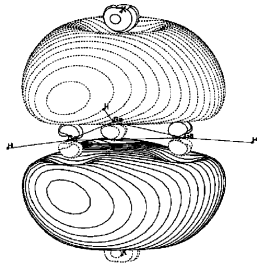

8

In spite of the aromatic $[cyclo\text{-}Ga_3]^{2-}$ anionic core found in **6**, the respective four-membered Ga_4 ring consists the core structure of a recently synthesized and structurally characterized organogallium molecule formulated as $K_2[Ga_4(C_6H_3\text{-}2,6\text{-}Trip_2)_2$ (Trip = C_6H_2-2,4,6-$^iPr_3$), **9** [125].

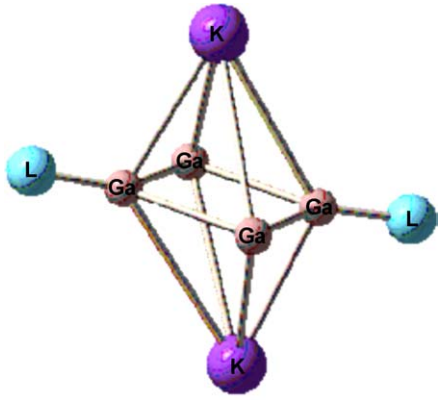

9: L= C_6H_3-2,6-$Trip_2$ (Trip = C_6H_2-2,4,6-$^iPr_3$),s

10: L = Ph

The structure of **9** is centrosymmetric with a planar, almost square Ga_4 core. The structure is completed with two K^+ ions on either side of the Ga_4 plane. DFT calculations at the B3LYP/LANL2-DZ level of theory on the model system $K_2[Ga_4Ph_2]$, **10** illustrated that the all-planar structure is a true minimum in the PES, while the nonplanar one containing a square planar Ga_4 core perpendicular to the two phenyl groups is a second order saddle point [126]. The bonding in **9** and **10** was interpreted on the grounds of the relevant MOs which describe the four-center π-bond and the three σ(Ga–Ga) bonds. Both **9** and **10** possessing two delocalized π electrons exhibit aromatic character conforming to the $4n + 2$ ($n = 0$) Hückel rule of aromaticity.

6. Aromatic metal clusters

A number of bare honometallic and bimetallic clusters as well as molecular metal cluster compounds either neutral or ionic were found recently to constitute novel classes of inorganic and organometallic compounds exhibiting a particular "type" of aromaticity, the so-called *metallaromaticity*. They can be divided roughly into two large classes: (i) the Zintl type anions with the general formula $A_n[M_m]$, which are negatively charged polyatomic clusters $[M_m]^{n-}$ of main-group metallic and/or semimetallic elements that are surrounded by various countercations A^+, particularly alkali metal cations and (ii) the ligand-stabilized cluster compounds of the general formula $[M_nL_m]$ which contain solely ligand-bearing metal atoms with the ligands L being either terminal or bridging adjacent metal atoms.

6.1. All-metal aromatic molecules

Recently the applicability of the aromaticity concept has been expanded to metallic clusters in a combined photoelectron spectroscopy and electronic structure computational investigation of all-metal molecules containing $[Al_3]^-$, $[Ga_3]^-$, $[XAl_3]^-$, $[Al_4]^{2-}$, $[Ga_4]^{2-}$, $[In_4]^{2-}$, $[Hg_4]^{6-}$, $[Al_5]^-$ and $[Al_6]^{2-}$ aromatic units [126–133]. All these systems are electron deficient species compared to the corresponding aromatic hydrocarbons. The electron deficiency results in an interesting new feature in metallic aromatic systems, which should be considered as having both π- and σ-aromaticity, and that should result in their additional stability. Boldyrev and Wang in a feature article published in *J. Phys. Chem. A* [134] surveyed their pioneering work on the design and characterization of a number of nonstoichiometric molecular and cluster species.

The simplest metal cluster exhibiting aromatic character is *cyclo*-$[Li_3]^+$ which adopts a triangular structure as its global minimum [135]. DFT and CCSD(T) calculations using the 6-311+G(d) basis set on a selected group of cationic, anionic and neutral triatomic and tetraatomic alkali metal and alkaline earth metal clusters were used to explain the planarity and relative stability of the clusters [133]. All these clusters having only valence s-AOs are expected to possess σ-aromaticity. Thus, *cyclo*-$[Li_3]^+$ cluster has only one completely delocalized bonding σ-MO constructed from the sum of the 2s-AOs of the three Li atoms of the three-membered metallic ring, which closely resembles the respective π-MO of the aromatic cyclopropenium cation $[C_3H_3]^+$. In the framework of the VB theory σ-aromaticity can be expressed by the resonance of three classical structures (Fig. 1) with one 2c–2e Li–Li bond.

The σ-resonance energy in the *cyclo*-$[Li_3]^+$ cation calculated as the energy difference between the Li_3Cl aromatic molecule and the Li_2 and LiCl reference molecules was predicted to be 35.7 kcal/mol at the highest level of theory. It was suggested that the electron-counting rule for σ-aromaticity is $4n + 2$ if only the s-AOs participate in the bonding. Obviously, for σ-antiaromaticity the electron-counting rule is $4n$. Based on the electron-counting rule $[Li_3]^-$ having four σ electrons would be expected to be a σ-antiaromatic system. It undergoes a Jahn–Teller distortion, thus enforcing the system to adopt a linear configuration [135]. The next species exhibiting σ-aromaticity is the bimetallic Li_2Mg_2 cluster having six σ electrons. The cyclic σ-aromatic structures of Li_2Mg_2 were predicted to be more stable than the linear Li–Mg–Mg–Li structure, thus showing the importance of aromaticity in metal clusters.

More recently, Kuznetsov and Boldyrev [136] using electronic structure calculation methods at the B3LYP/6-311+G(d) and CCSD(T)/6-311+G(2-Df) levels predicted that in the bimetallic $[NaMg_3]^-$ and $[Na_2Mg_3]$ clusters the basic structural unit is an unusual $[Mg_3]^{2-}$ trigonal planar cluster exhibiting an extraordinary "type" of π-aromaticity without initial formation of the σ-framework. The π-aromaticity of $[Mg_3]^{2-}$ equilateral triangle was further substantiated by the NICS criterion of aromaticity calculated at the B3LYP/6-311+G(d) level of theory. The high NICS(0) values of −30.4 and −29.8 ppm for $[Mg_3]^{2-}$ and $[Na_2Mg_3]$ clusters, respectively indicate the high aromatic character of the species. Notice that the NICS(0) value for the aromatic cyclopropenium cation $[C_3H_3]^+$ is −22.4 ppm at the B3LYP/6-31G(d, p) level of theory. The binding energies of the two most external electrons in the most stable [*cyclo*-$Mg_3]^{2-}$ (D_{3h}) cluster computed at the gradient-corrected DFT incorporating a new scheme for converting the Kohn–Sham eigenvalues into electron removal energies was found to be 0.140 eV/atom [137].

The electronic structure and stability of $[Be_5]^{0,+,-}$ clusters have been studied very recently [138] at the B3LYP, B3PW91, and MP2 levels of theory. The global minimum for the $[Be_5]^{0,+,-}$ clusters corresponds to the trigonal bipyramidal structure with D_{3h} symmetry. It should be noted that the prolate structures of $[Be_5]^{0,+,-}$ clusters are also predicted by the ellipsoidal jellium model (EJM) for electron counts of $n = 9$, 10 and 11 [65]. In all clusters there is a strong electron delocalization that enhances their stability, and the computed NICS(0) values (−22.3, −46.5 and −54.6 ppm for the anionic, neutral and cationic Be_5 clusters, respectively) indicate a relatively strong aromatic character with the cationic species having the stronger aromaticity. The isomeric species

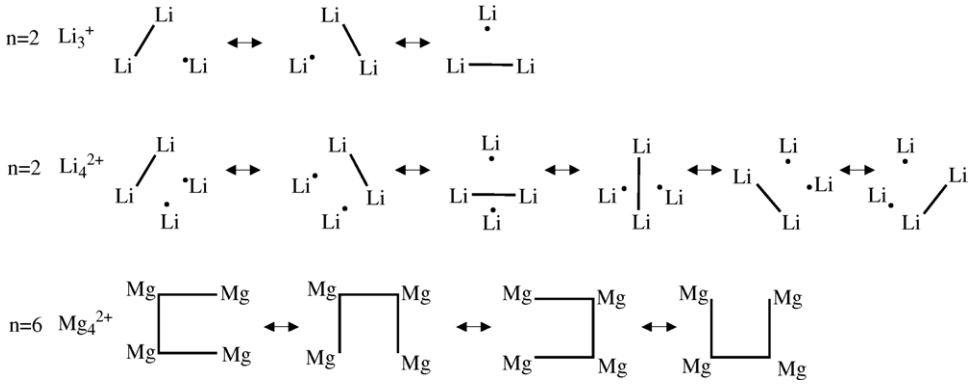

Fig. 1. Resonance structures of $[Li_3]^+$, $[Li_4]^{2+}$ and $[Mg_4]^{2+}$. Reproduced with permission from [133]. Copyright by the American Chemical Society.

having the planar pentagon structure were also located on the PES as local minima. The neutral and cationic species were predicted to be antiaromatic, while the anionic one is nonaromatic. The $[Be_3]^-$ adopts the trigonal planar configuration with D_{3h} symmetry which is stabilized by the relaxation and correlation energies at the CCSDT level of theory [139]. The equilateral triangular structure is also adopted by the *cyclo*-$[B_3]^-$, *cyclo*-$[Al_3]^-$, and *cyclo*-$[Ga_3]^-$ anions and the neutral gas phase Na[B_3], Na[*cyclo*-Al_3], and Na[*cyclo*-Ga_3] molecules [132]. The triangular *cyclo*-$[B_3]^-$, *cyclo*-$[Al_3]^-$, and *cyclo*-$[Ga_3]^-$ anions possess two delocalized π electrons and are aromatic.

In their pioneering work Li et al. [127] reported the most convincing experimental and theoretical evidence of aromaticity in an all-metal system the *cyclo*-$[Al_4]^{2-}$ ion in a series of bimetallic and ionic clusters, M[*cyclo*-$Al_4]^-$ (M = Li, Na, or Cu). All these species as well as the Ga and In analogues [126] have been created through a laser vaporization and have been studied with negative ion photoelectron spectroscopy measurements and ab initio calculations. An Al/Cu (or Na and Li) alloy is hit with an intense pulsed laser that vaporizes a small amount of the target instantly. A helium carrier gas then mixes with the metal vapor, and initiates nucleation or cluster formation. These molecules are normally prepared as singly charged anions because doubly charged species are expected to be rather unstable in the gas phase due to strong intramolecular Coulomb repulsion. Obviously, complexation with counterions is required to produce more stable species and is also convenient for mass analysis and photodetachment experiments. All the M[*cyclo*-$Al_4]^-$ species possess a pyramidal structure containing a M^+ cation interacting with a square planar [*cyclo*-$Al_4]^{2-}$ unit. The excellent agreement between the calculated photoelectron spectra for the pyramidal structures and the experimental spectra lends considerable support to the idea that the pyramidal structures are the global minimum for the M[*cyclo*-$Al_4]^-$ species. The high planarity and bond length equalization of the square planar [*cyclo*-$Al_4]^{2-}$ unit are indicative of aromaticity which subsequently was verified by magnetic and electronic criteria, as well.

Ab initio and DFT computational techniques were used to determine the equilibrium structures of a series of all-metal anionic M[*cyclo*-$M'_4]^-$ (M = Li, Na, or Cu, M′ = Al, Ga, or In) and neutral M_2[*cyclo*-$M'_4]^-$ (M = Li, Na, or Cu, M = Al, or Ga) aromatic molecules [127,128,130]. It was found that the most stable structure (global minimum) for all three M[*cyclo*-$Al_4]^-$ species is a square pyramid consisting of an M^+ cation coordinated to a square planar *cyclo*-$[Al_4]^{2-}$ unit. On the other hand, the singlet structures with one Na^+ cation coordinated to the face and another to the edge of the square-planar *cyclo*-$[M'_4]^-$ dianions in the neutral M_2[*cyclo*-$M'_4]^-$ clusters were found to be the global minima. Even though the *cyclo*-$[Al_4]^{2-}$ dianion was not expected to be thermodynamically stable toward autodetachment of an electron it was anticipated that metastable local minima could be located on the PES. The equilibrium structure of the *cyclo*-$[Al_4]^{2-}$ dianion is perfectly planar and seems to undergo very little structural changes in forming the M[cyclo-$M'_4]^-$ and M_2[*cyclo*-$M'_4]^-$ molecules. It is important to be noticed that the oblata (flat) structure of the *cyclo*-$[Al_4]^{2-}$ dianion corresponding to the electron-count (magic number) of $n = 14$ is predicted by the EJM model, thus accounting for its high stability [65].

The *cyclo*-$[Al_4]^{2-}$ dianion, both as an isolated species and in the bimetallic clusters, was found to be square-planar and to posses a doubly occupied delocalized a_{2u} π-MO, thus conforming to the $(4n + 2)$π-electron-counting rule for aromaticity. The cyclic delocalization of the 2π electrons was found to be responsible for the planar structure and aromaticity of the *cyclo*-$[Al_4]^{2-}$ unit. The relevant valence molecular orbitals are depicted schematically in Fig. 2.

It can be seen that the highest occupied molecular orbital (HOMO) is a delocalized π orbital of a_{2u} symmetry corresponding to π-bonding; the rest of the MOs are either σ-type bonding or lone pairs. Four MOs namely HOMO-3 ($1b_{1g}$), HOMO-4 ($1e_u$) and HOMO-5($1a_{1g}$) correspond to Al lone pairs, while two MOs, the HOMO-1($2a_{1g}$) and HOMO-2($1b_{2g}$) correspond to σ-bonding. All three bonding MOs are completely bonding-delocalized orbitals, and therefore they all should add extra stability to the all-metal aromatic system. Such double or triple aromaticity (if two σ bonds are

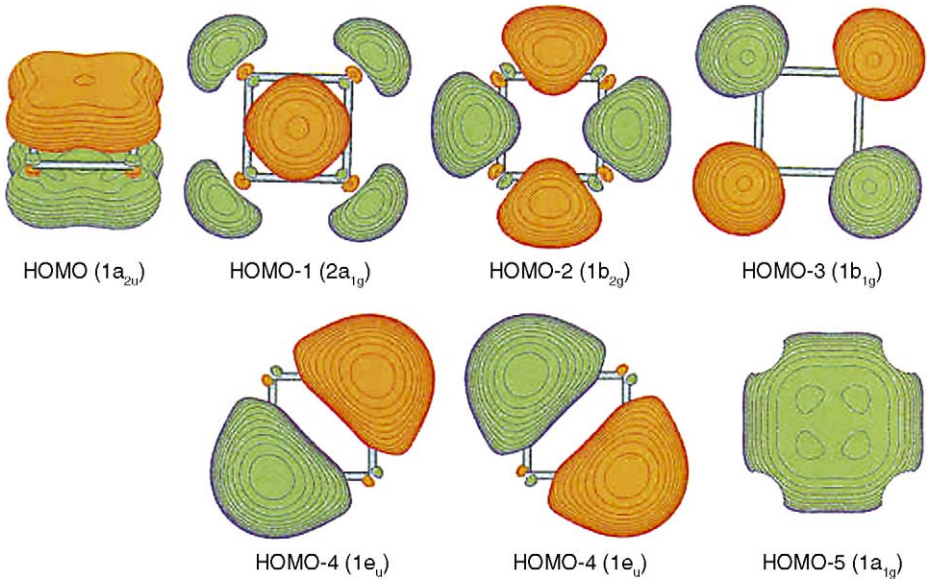

Fig. 2. Molecular orbital pictures of square planar *cyclo*-$[Al_4]^{2-}$, showing the HOMO ($1a_{2u}$) down to the fifth valence molecular orbital from the HOMO (HOMO-5, $1a_{1g}$). HOMO-4 consists of a degenerate pair ($1e_u$). Reproduced with permission from [127]. Copyright [2001] AAAS.

considered separately) should result in much higher "resonance" or stabilization energy in *cyclo*-$[Al_4]^{2-}$ which has been recognized as a prototype of a new class of aromatic molecules. In fact, Boldyrev and kuznetsov [130] performing B3LYP/6-311 + G(d) and CCSD(T)/6-311 + G(2-Df) calculations on the Na_2[*cyclo*-Al_4] and Na_2[*cyclo*-Ga_4] aromatic molecules obtained crude evaluations of their relatively high resonance energies; 48 and 20 kcal/mol, respectively at the B3LYP/6-311+G(d) level of theory compared to 20 kcal/mol in benzene.

Zhan et al. [140] using high-level ab initio calculations at the CCSD(T)/aug-cc-pVxZ (x = D, T and Q) level of theory and extrapolating to the complete basis set limit calculated the first electron affinities of Al_n (n = 0–4) clusters and estimated their resonance energies which were found to be quite large (∼72.7 kcal/mol as the upper limit or ∼52.5 kcal/mol as the lower limit). They concluded that the *cyclo*-$[Al_4]^{2-}$ species exhibits a "3-fold" aromaticity due to the presence of three independent delocalized bonding systems, one pure π-bonding system and two σ-bonding systems all satisfying the $4n + 2$ electron-counting rule of aromaticity. In the framework of the valence bond (VB) theory the electronic structure of the *cyclo*-$[Al_4]^{2-}$ aromatic species can be represented by $4 \times 4 \times 4 = 64$ potential resonating Kekulé-like structures with each structure having three localized chemical bonds. On the other hand, the *cyclo*-$[Al_3]^{-}$ aromatic species exhibits a "2-fold" aromaticity (one π and one σ) which can be represented by $3 \times 3 = 9$ potential resonating Kekulé-like structures, each with two localized chemical bonds. Along this line Zhan et al. [140] suggested that a molecular system either organic or inorganic could have multi-fold aromaticity depending on the particular delocalized bonding system satisfying a certain electron-counting rule of aromaticity.

Very recently Havenith and van Lenthe [141] performed ab initio valence bond calculations in order to assess the σ and π aromatic character of the *cyclo*-$[Al_4]^{2-}$ species. They found that the σ electronic system is composed from two independent systems resulting from the interaction of the radial and tangential p-AOs, respectively. Both systems contain two delocalised electrons and are responsible for the conduction. The computed resonance energy of the σ electronic system found to be 123 kcal/mol is significantly higher than that of the π electronic system (40 kcal/mol). The resonance energy of the corresponding π electronic system of the isoelectronic aromatic cyclobutadiene dication $[C_4H_4]^{2+}$, was found to be much higher (167 kcal/mol).

Although the first motivation for proposing aromaticity of the *cyclo*-$[Al_4]^{2-}$ species was based on the $(4n + 2)$π-electron-counting rule of aromaticity, direct visualization of the induced current density using the *ipsocentric* CTOCD-*DZ* approach pinpoints the induced diatropic ring current here as an essentially σ effect, with little or no contribution from the π electrons [142]. Both the induced σ diatropic ring current and other indicators of aromaticity of the aromatic *cyclo*-$[Al_4]^{2-}$ species remain essentially unchanged in the pyramidal M[*cyclo*-Al_4]$^-$ species. More recently, Fowler and co-workers [16] using the *ipsocentric* CTOCD-*DZ* approach computed the magnetic-field induced current density maps for a series of Li_x[*cyclo*-Al_4] (x = 0–4) clusters. Perusal of the total (σ + π) and π current density maps (Fig. 3) and their breakdown into orbital contributions (Fig. 4) for the *cyclo*-$[Al_4]^{2-}$, Li[*cyclo*-Al_4]$^-$ and Li_2[*cyclo*-Al_4] aromatic molecules revealed that the ring current in these three "2π"-electron systems is strongly σ-dominated, and therefore these systems should be qualified as four-electron σ-aromatics and not at all as π-aromatics. Moreover, the π-electron counts

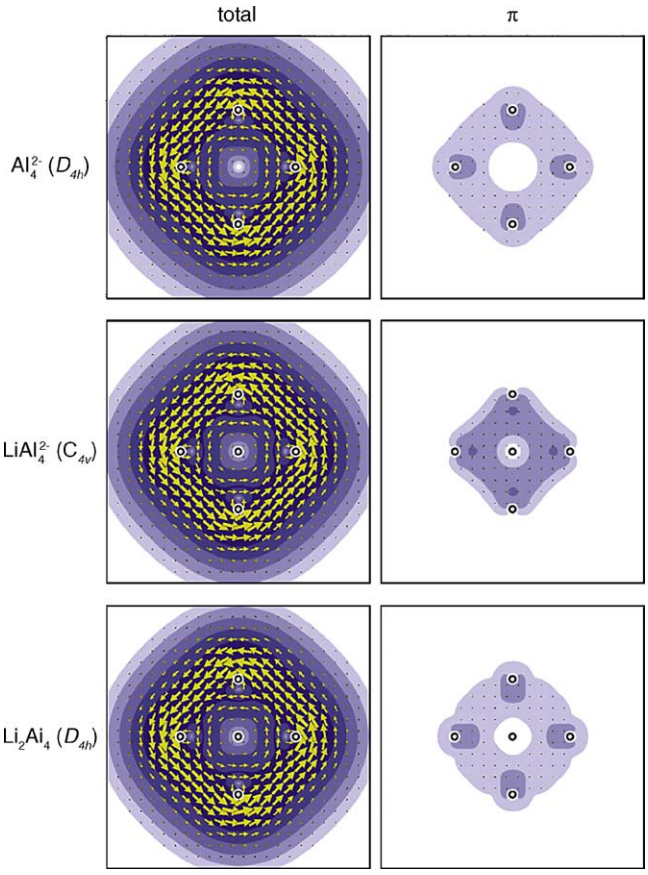

Fig. 3. The total ($\sigma + \pi$) and π-only current densities induced by a magnetic field directed along the principal axis in *cyclo*-$[Al_4]^{2-}$ (D_{4h}), Li[*cyclo*-Al_4]$^-$ (C_{4v}) and Li_2[*cyclo*-Al_4] (D_{4h}) species. Circles mark the nuclear positions projected on the plotting plane, arrows depict the in-plane projection of current, and contours show the magnitude of the total current, all referred to a height $1a_0$ above the Al_4 plane (i.e., towards Li in Li[*cyclo*-Al_4]$^-$) [16]. Reproduced by permission of the PCCP Owner Societies.

of 2 and 4 in the Li_x[*cyclo*-Al_4] clusters are associated with 2 magnetically inactive π-electrons, or 2 active and 2 inactive π-electrons. Schleyer and co-workers [143] based on a new refinement of NICS analysis characterizing the magnetic character of each canonical MO (CMO) individually abbreviated as CMO-NICS analyses found that the Li_3[*cyclo*-Al_4]$^-$ species are aromatic rather than antiaromatic, due to the predominant effects of σ-aromaticity over π-anti-aromaticity.

More recent theoretical investigations [144] revealed that the *cyclo*-$[Al_4]^{2-}$ unit in the neutral Na_4[*cyclo*-Al_4] and anionic Na_3[*cyclo*-Al_4]$^-$ clusters exhibits a rectangular structure with alternate π bonds. These species have $4n$ π electrons and therefore are metallo-antiaromatic compounds.

Very recently, Datta and Pati [145] investigated the linear and nonlinear electric polarizabilities of small Al_4M_4 (M = Li, Na, and K) clusters. It was found that these $[Al_4]^-$ clusters functionalized with various metal cations possess an exceptionally high magnitude of linear and nonlinear coefficients, which are orders of magnitude higher than the conventional π-conjugated systems of similar sizes. The alkali atoms surrounding the ring introduce a noncentrosymmetricity in the systems that leads to charge transfer with small optical gap and low bond length alternation. The low bond length alternation is indicative of aromaticity in these clusters and along with the large NLO coefficients they appear to be better candidates for next generation NLO fabrication devices.

Sandwich-like complexes based on *cyclo*-$[Al_4]^{2-}$ aromatic compounds with structures similar to that of metallocenes have recently been reported by Mercero and Ugalde [146] using DFT computational techniques. They found that the $[Al_4TiAl_4]^{2-}$ sandwich-like complex adopts a staggered configuration with D_{4d} symmetry. The computed electron detachment energies (EDE) indicated that the monoanion is more stable than the dianion. Moreover, the large binding energy around 610 kcal/mol indicates that fragmentation of the molecule is not possible and the sandwich-like molecule exhibits relatively strong aromatic character reflected on the high negative NICS(0) value of -39 ppm, as compared to the NICS(0) value of the "free" *cyclo*-$[Al_4]^{2-}$ species (-28 ppm).

The structure and chemical bonding of a series of M$[Al_6]^-$ (M = Li, Na, K, Cu, and Au) bimetallic clusters have been investigated by a combination of photoelectron spectroscopy

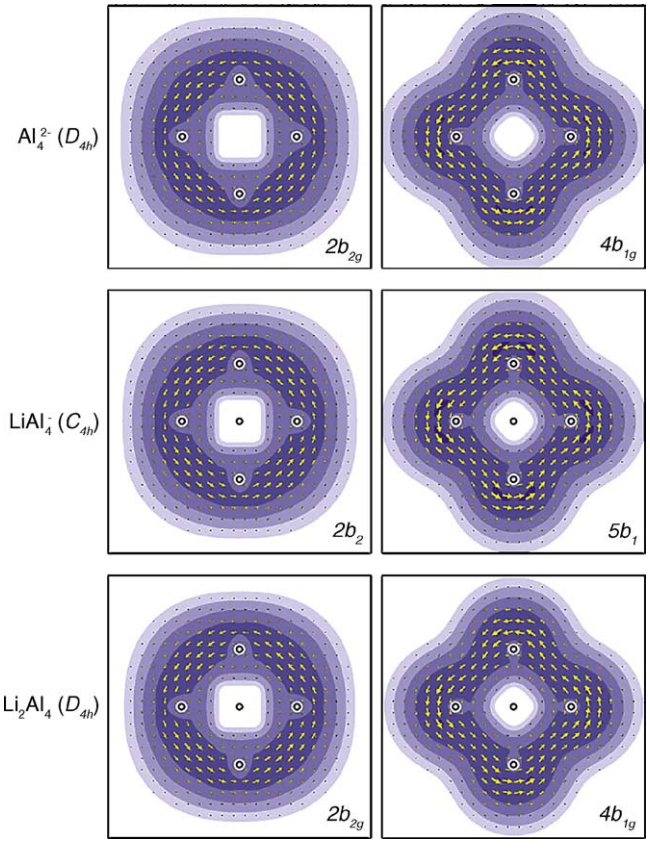

Fig. 4. The main orbital contributions to the σ ring current of *cyclo*-$[Al_4]^{2-}$ (D_{4h}), Li[*cyclo*-Al_4]$^-$ (C_{4v}) and Li_2[*cyclo*-Al_4] (D_{4h}) species. Plotting conventions as Fig. 3 [16]. Reproduced by permission of the PCCP Owner Societies.

and electronic structure calculation methods [131]. It was found that all $M[Al_6]^-$ clusters possess a C_{3v} ground-state structure derived from the O_h structure adopted by the $[Al_6]^{2-}$ cluster. A detailed MO analysis revealed that the $[Al_6]^{2-}$ dianion can be viewed as the fusion of two aromatic [*cyclo*-$Al_3]^-$ anions. Interestingly, every face of the $[Al_6]^{2-}$ octahedron still possesses both σ- and π-aromaticity analogous to that of the [*cyclo*-$Al_3]^-$ monomeric species and therefore it can be viewed to render three-dimensional aromaticity with a large stabilization energy.

The aromaticity concept was further extended to heterocyclic [*cyclo*-$XAl_3]^-$ (X = Si, Ge, Sn, Pb) clusters which are isoelectronic to [*cyclo*-$Al_4]^{2-}$ aromatic molecule [129]. The [*cyclo*-$MAl_3]^-$ species were produced by laser vaporization of the respective alloy targets and analyzed by using time-of-flight mass spectrometer. Electronic structure calculations at the B3LYP and CCSD(T) levels of theory illustrated that all [*cyclo*-$XAl_3]^-$ species have two lowest singlet isomers: a four-membered heterocyclic structure of C_{2v} symmetry and a pyramidal structure of C_{3v} symmetry (Fig. 5). It was found that the most stable structure of all four [*cyclo*-$XAl_3]^-$ species is the C_{2v} cyclic structure. The stability of the C_{2v} cyclic structure relative to the pyramidal one is related to the HOMO-1 ($1b_1$) for [*cyclo*-$SiAl_3]^-$ and [*cyclo*-$GeAl_3]^-$, and HOMO ($1b_1$) for [*cyclo*-$SnAl_3]^-$ and [*cyclo*-$PbAl_3]^-$, which correspond to a delocalized π orbital. The heterocyclic structure was found to possess aromaticity with two delocalized π-electrons, analogous to that of the [*cyclo*-$Al_4]^{2-}$ aromatic species. The nature of heteroatom X affects the cyclic π-electron delocalization and consequently the stability of the heterocyclic [*cyclo*-$XAl_3]^-$ ring.

The electronic structure and chemical bonding of anionic tetrapnictogen $[Pn_4]^-$ and pentapnictogen $[Pn_5]^-$ (Pn = P, As, Sb and Bi) clusters were investigated using both photoelectron spectroscopy and electronic structure calculation methods [147,148]. The tetrapnictogen $Na^+[Pn_4]^{2-}$ anions contain an aromatic [*cyclo*-$Pn_4]^{2-}$ dianion, while the $Na^+[Pn_4]^-$ neutral species contain an antiaromatic [*cyclo*-$Pn_4]^-$ anion. Two types of antiaromatic structures were characterized; the conventional rectangular structure and a new peculiar rhombus one [147]. All pentapnictogen $[Pn_5]^-$ species exhibit the aromatic cyclic singlet structure of D_{5h} symmetry as their ground state with a low-lying isomer of C_{2v} symmetry. The latter gains stability along the series [*cyclo*-$P_5]^- <$ [*cyclo*-$As_5]^- <$ [*cyclo*-$Sb_5]^-$. The valence shell molecular orbital pattern of the aromatic [*cyclo*-$Pn_5]^-$ molecules resemble that of the aromatic cylopentadiene anion except that the MO ordering is slightly different. In [*cyclo*-$Pn_5]^-$ molecules the most stable π-MO ($1a_{2''}$) lies below the σ-MOs, whereas in $[C_5H_5]^-$ all three π-MOs lie above the σ-MOs.

The aromatic [*cyclo*-$Sb_5]^-$ and [*cyclo*-$Bi_5]^-$ anionic ligands, the heavier counterparts of the cyclopentadienide (Cp) anion, and their metal-centered planar cationic [Fe(*cyclo*-$Sb_5)]^+$ and [Fe(*cyclo*-$Bi_5)]^+$ species have recently been investigated by Frenking and co-workers [149] using gradient-corrected DFT at the BP86/TZ2P level of theory. Frenking's group extended the investigations to the group-15 analogues of metallocenes [Fe(η^5-$E_5)_2$], [FeCp(η^5-$E_5)$] and [Ti(η^5-$E_5)_2$] (E = P, As, Sb, Bi) [149–152]. It was predicted that all π-heterocyclic complexes are stable compounds, while the metal–ligand bonding, analyzed with an energy decomposition method, was shown to come from 53 to 58% electrostatic attraction and 42 to 47% from covalent interactions. The [Fe(*cyclo*-$Sb_5)]^+$ and [Fe(*cyclo*-$Bi_5)]^+$ species were predicted to have planar equilibrium geometries of D_{5h} symmetry with the Fe ion at the center of the pentagonal [*cyclo*-$Sb_5]^-$ and [*cyclo*-$Bi_5]^-$ anionic ligands (Fig. 6). Analysis of the molecular orbitals of the [Fe(*cyclo*-$Sb_5)]^+$ and [Fe(*cyclo*-$Bi_5)]^+$ species revealed that these novel aromatic

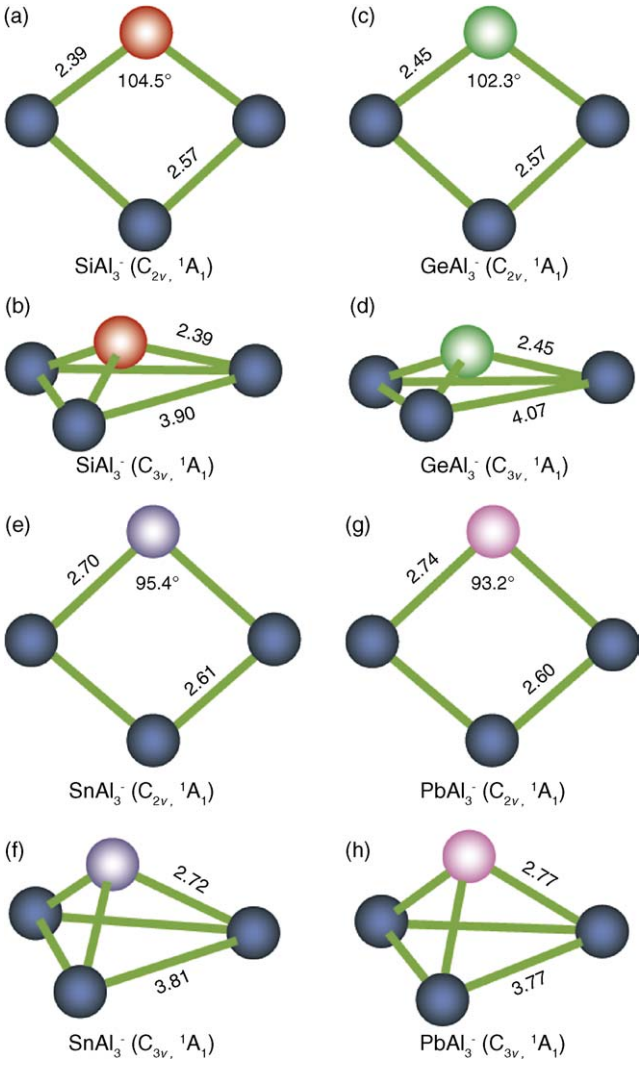

Fig. 5. Optimized structures of [*cyclo*-$XAl_3]^-$ at the CCSD(T)/6-311+G(d) and CCSD4s4p1d level of theory. Bond lengths are given in Å. (a) Cyclic planar [*cyclo*-$SiAl_3]^-$ (C_{2v}, $^1A_1$), (b) pyramidal $[SiAl_3]^-$ (C_{3v}, $^1A_1$), (c) cyclic planar [*cyclo*-$GeAl_3]^-$ (C_{2v}, $^1A_1$), (d) pyramidal $[GeAl_3]^-$ (C_{3v}, $^1A_1$), (e) cyclic planar [*cyclo*-$SnAl_3]^-$ (C_{2v}, $^1A_1$), (f) pyramidal $[SnAl_3]^-$ (C_{3v}, $^1A_1$), (g) cyclic planar [*cyclo*-$PbAl_3]^-$ (C_{2v}, $^1A_1$), and (h) pyramidal $[PbAl_3]^-$ (C_{3v}, $^1A_1$). Reproduced with permission from [129]. Copyright by the Wiley-VCH Verlag GmbH&Co. KgaA, Weinheim.

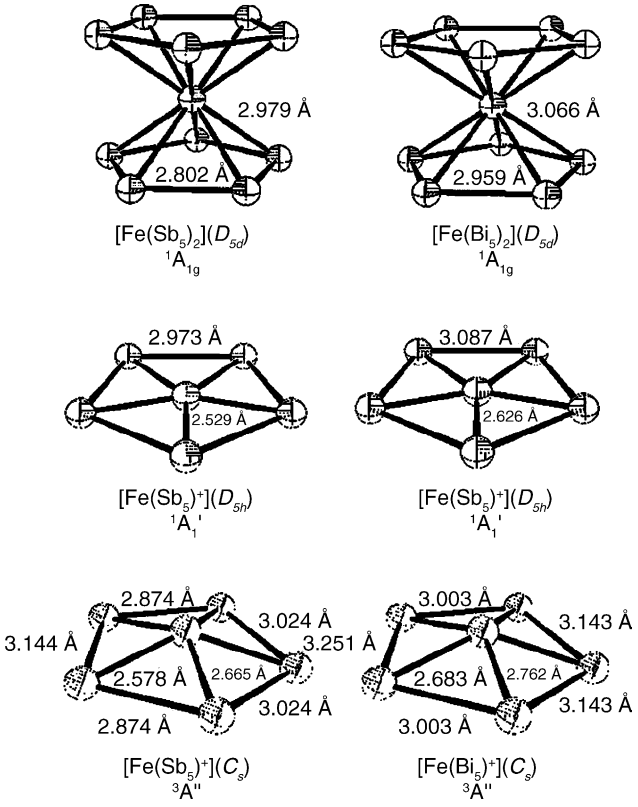

Fig. 6. Calculated of [Fe(*cyclo*-E_5)$_2$], [Fe(*cyclo*-E_5)]$^+$ and [*cyclo*-E_5]$^-$ (E = Sb, Bi) at BP86/TZ2P along with the symmetry groups and electronic configurations. All structures are minima on the PES. Reproduced in part with permission from [149]. Copyright by the Wiley-VCH Verlag GmbH&Co. KgaA, Weinheim.

transition-metal-centered molecules involve strong π bonds between the aromatic ring and the metal atom d(π) AOs. Energy decomposition analysis of the iron-ligand bonding illustrated that the Fe-E_5^+ bonding in both molecules is slightly more covalent than electrostatic. It is the π orbitals that make a very large contribution to the covalent term. Interestingly, the BP86/GIAO calculations predicted that the ^{57}Fe NMR chemical shifts of the aromatic [Fe(*cyclo*-Sb_5)]$^+$ and [Fe(*cyclo*-Bi_5)]$^+$ molecules are dramatically shifted towards much larger δ values indicating that the Fe nucleus is highly deshielded as a result of the induced diatropic ring current of the aromatic [*cyclo*-Sb_5]$^-$ and [*cyclo*-Bi_5]$^-$ ligands.

Five-membered aromatic rings, analogous to the cyclopentadienyl anion, have also been observed for the heavy metals of Sn and Pb. Thus, Todorov and Sevov [153] prepared and characterized the isostructural Zintl phases Na_8BaPb_6, Na_8BaSn_6, and Na_8EuSn_6, which contain isolated planar aromatic five-membered rings of [cyclo-Sn_5]$^{6-}$ and [cyclo-Pb_5]$^{6-}$, which are the first aromatic species of such heavy metals.

Recent years have witnessed increased interest in gold-containing nanostructures, as they have found far-reaching applications in areas such as catalysis, sensors, molecular electronics, or as bioconjugate probes for application tags in gene analysis, antibody, or gene mapping [154]. An extensive DFT study of the electronic structure and bonding in anionic coinage metal clusters, focusing on $[Cu_7]^-$, $[Ag_7]^-$, and $[Au_7]^-$ indicated that $[Au_N]^-$ clusters favor planar structures (with *N* as large as 13) as a result of strong hybridization of the atomic 5d and 6s orbitals due to relativistic effects [155,156]. Interestingly, according to recent studies by Häkkinen and Landman [157] as well as by Bravo-Pérez et al. [158] Au_6 prefers a trigonal planar D_{3h} structure (Fig. 7), which is lower in energy than the other possible arrangements including the octahedral one. The preferred planarity of small gold clusters is attributed to relativistic effects [155]. However, it is worthwhile to think that aromaticity should also be responsible for the planarity of the $[Au_N]^-$ clusters. The structural and electronic properties of bimetallic silver–gold clusters have been thoroughly investigated by Bonačić-Koutecký et al. [159] using DFT computational techniques. It was found that the bimetallic tetramer and hexamer silver–gold clusters are planar, while the heteronuclear bonding is usually preferred to homonuclear one in clusters with equal numbers of heteroatoms. Again it is worthwhile to use some of the aromaticity criteria to prove whether the planar structures exhibit aromatic character or not.

The structures of small gold cluster cations ($[Au_n]^+$, $n < 14$) [160] and anions [161] were determined by a combination of ion mobility measurements and DFT calculations. From the comparison of the experimental cross sections with the DFT results, structural assignments have been made indicating that room temperature gold cluster cations are planar up to $n = 7$, while starting from $n = 8$ 3D structures that in most cases can be thought of as slightly distorted fragments of the bulk lattice structure are formed [160]. On the other

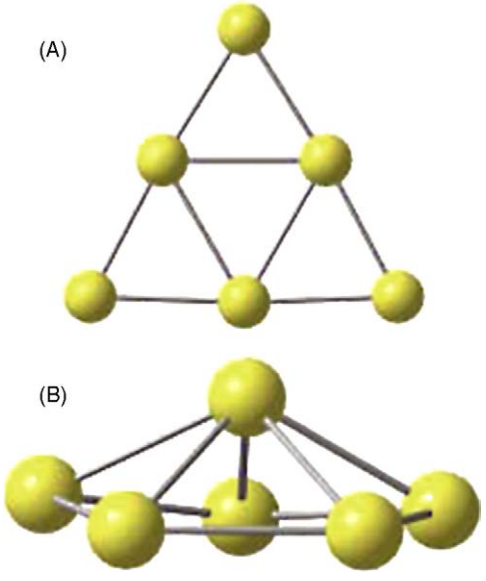

Fig. 7. Low energy minimum structures of Au_6: (A) trigonal planar (global minimum), (B) distorted pentagonal pyramid. Reproduced with permission from [154]. Copyright by the Wiley-VCH Verlag GmbH&Co. KgaA, Weinheim.

hand, by comparisons of the DFT results with the measured collision cross sections, as well as the vertical detachment energies (VDEs), the structures of the small $[Au_n]^-$ ($n < 13$) anions were assigned and the transition from 2D to 3D structures was found to occur at an unusually large cluster size of twelve gold atoms [161]. Aromaticity seems to provide a plausible explanation for this anomalous behavior of gold. The geometrical and electronic structures of neutral gold and silver clusters (Au_k, Ag_k, $k = 1$–13), and neutral and anionic gold–silver binary clusters (Au_mAg_n, $2 \leq k = m + n \leq 7$) have extensively been investigated using DFT and high level ab initio calculations including coupled cluster theory with relativistic ab initio pseudopotentials [162]. The Au_k and Ag_k clusters show the odd-even oscillation for their stability and electronic properties as a function of the atoms. In the neutral state, even numbered k tends to be more stable, while in the anionic state, odd numbered k tends to be more stable. This is in line with the predictions of the EJM model. Overall, in the neutral clusters gold favors 2D structures, while silver favors 3D structures from $k = 7$ up to $k = 13$. In the anionic clusters, the lower dimensional preference is strengthened, and so the 2D preference is much more pronounced in both gold and silver. In the binary clusters (alloys) the structures are strongly correlated to the pure gold and silver structures, depending on the ratio of the number of gold to silver atoms in the cluster. It was also found that in the binary clusters there is a charge transfer from gold to silver which provides significant electrostatic stabilization, thus making the alloy formation more favorable than pure gold and silver clusters.

More recently, Fernández et al. [163] reported on a systematic study of the structure and electronic properties of noble metal clusters $[X_n]^\nu$ (X = Cu, Ag, Au; $\nu = -1$, 0, +1; $n \leq 13$ and $n = 20$) using DFT computational techniques. The anionic, neutral and cationic gold clusters adopt planar ground-state structures with up to 12, 11, and 7 gold atoms, respectively. On the other hand, silver clusters adopt planar structures for maximum number of atoms 5, 6, and 5 for anionic, neutral and cationic clusters, respectively, while copper clusters form planar structures for maximum number of atoms 5, 6, and 4 for anionic, neutral and cationic clusters, respectively. The predicted planarity of the gold clusters was in line with the expectations from ion mobility measurements and calculations for cationic [160] and anionic [161] gold clusters and with photoelectron spectra [156]. The tendency to planarity of gold clusters, which is much larger than in silver and copper, was attributed to relativistic effects, which decrease the s-d promotion energy and lead to hybridization of the half-filled 6s AO with the fully occupied $5d_z2$ AO. In the framework of the "simple" s-electron alkali metals, electronic shell model stabilization and magic numbers were found to be adequate concepts for Ag and Cu clusters, but not for Au clusters in the range of the sizes studied. The electronic properties of the clusters, such as cohesive energy, ionization potentials, electron affinities and HOMO–LUMO gap were rationalized in terms of 2D and 3D electronic shell models. For the Au_{20} cluster the predicted ground state structure exhibits T_d symmetry, while the Ag_{20} and Cu_{20} clusters adopt a compact C_1 structure in partial agreement with the calculations by Wang et al. [164], who find a T_d structure also for the Ag_{20} cluster. The latter authors predicted large HOMO–LUMO gap for Au_{20} and Ag_{20} clusters with T_d structures, but much smaller for Cu_{20} with similar structure.

The recent observation of the Au_{20} cluster [165] generated by the laser vaporization of a pure gold target with a helium carrier gas, prompted King et al. [166] to study the structure and bonding using electronic structure calculation methods at the B3LYP level of theory. The Au_{20} cluster adopts an omnicapped truncated tetrahedral structure, which can be generated from a regular dodecahedron by forming two transannular Au–Au bonds across each face preserving the T symmetry. The spherical harmonic MO pattern of $Au_{20}(T_d)$ cluster is similar to that in other deltahedral clusters exhibiting spherical aromaticity. The chemical bonding analysis and computations indicated that $Au_{20}(T_d)$ is a stable aromatic gold cluster, which may be possible to isolate as a discrete molecular species. In effect, the aromatic $Au_{20}(T_d)$ cluster coordinated with eight PPh_3 ligands has very recently been synthesized and its composition and molecular weight were confirmed by the isotopic pattern and accurate measurements of its doubly charged cation [167]. Collision-induced dissociation (CID) experiments revealed that four PPh_3 ligands are easily removed from the $[Au_{20}(PPh_3)_8]^{2+}$ dication yielding a highly stable $[Au_{20}(PPh_3)_4]^{2+}$ dication. High resolution UV-photoelectron spectra of cold mass selected $[Cu_n]^-$, $[Ag_n]^-$, and $[Au_n]^-$ clusters with $n = 53$–58 were measured very recently by Häkkinen et al. [168]. It was found that the observed electron density of states (DOS) is not compatible with the simple electron structure, but is strongly influenced by electron-lattice interactions. $[Cu_{55}]^-$ and $[Ag_{55}]^-$ clusters exhibit highly degenerate states as a consequence of their icosahedral symmetry, while $[Au_{55}]^-$ cluster shows drastically different spectra with almost no degeneracy. This provides strong evidence that the $[Au_{55}]^-$ cluster does not adopt icosahedral or cuboctahedral symmetry, but prefers a low-symmetry structure as a result of relativistic effects. Structural patterns of unsupported gold clusters have been identified using DFT computational techniques [169]. It was found that even "magic" cluster sizes exhibiting very compact and symmetric structures have also lower-energy distorted structures, the so-called "amorphous" structures. The origin of these structures was shown to lie in the non-pairwise metallic interactions. Wilson and Johnston [170] modeling gold clusters with an empirical many-body potential using molecular dynamics simulated annealing (MDSA) identified four distinct structural motifs for the structures of the predicted global minima, based on octahedral, decahedra, icosahedra and hexagonal prisms. It seems to be interesting to study spherical aromaticity in these highly symmetric structures using magnetic and electronic criteria.

Bimetallic Cu–Au nanoalloy clusters with up to 56 atoms have been studied by Johnston et al. [171] using a genetic algorithm. The global minima of the bimetallic clusters

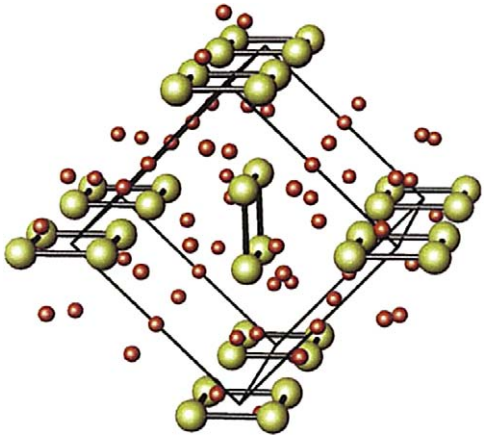

Fig. 8. Crystal structure of Na_3Hg_2, showing the Hg_4 square units (yellow) surrounded by Na (red). Reproduced with permission from [128]. Copyright by the Wiley-VCH Verlag GmbH&Co. KgaA, Weinheim. (For interpretation of the references to color in this figure legend, the reader is referred to the web version of the article.)

correspond to structures based on icosahedral packing. The $[CuAu]_M$ and $[CuAu_3]_M$ clusters tend to have layered arrangements of Cu and Au atoms, whereas the Cu and Au atoms are noticeably more mixed in the $[Cu_3Au]_M$ clusters. More recently [172], a new family of "magic" cluster structures of bimetallic Ag–Ni and Ag–Cu nanoparticles were found by genetic global optimization and DFT calculations. These bimetallic clusters involve an inner Ni or Cu core and an Ag external shell, as experimentally observed for Ag–Ni, and exhibit a polyicosahedral character with high-symmetry, large HOMO–LUMO energy gaps and remarkable structural, energetic and electronic stability, which could probably be attributed to spherical aromaticity of the clusters.

Johansson et al. [173] using scalar relativistic DFT calculations showed that the Au_{32} cluster has a local minimum corresponding to an icosahedral fullerenic form composed of triangles in icosahedral symmetry, making a near perfect rhombic triacontahedron. The diameter of the fullerenic Au_{32} cluster being about 0.9 nm, matches the most common diameter of the stable nanotubes reported previously by Kondo and Takayanagi [174]. Interestingly, the 24-carat golden fullerene has a record value of magnetic shielding at its center (NICS(0) = −100 ppm), and therefore exhibits a strong aromatic character. The Au_{32} cluster having 32 6s electrons of gold conforms to the $2(N+1)^2$ ($N=3$) electron-counting rule for spherical aromaticity.

Last but not least is the recent report [128] on a class of amalgams that contain [*cyclo*-Hg_4]$^{6-}$ square units as their building blocks, typified by that found in solid Na_3Hg_2 (Fig. 8).

The [*cyclo*-Hg_4]$^{6-}$ unit is isoelectronic with the [*cyclo*-Al_4]$^{2-}$ cluster, suggesting that the former is aromatic as well, thus explaining its unique stability and structure. An analysis of the MOs of the perfectly square planar [*cyclo*-Hg_4]$^{6-}$ species reveal that its structural and electronic stability should be attributed not only to π-aromaticity due to the presence of the two π electrons in the $1a_{2u}$ MO, but also to σ-aromaticity due to the occupation of the two four-center σ-bonding MOs, $1b_{2g}$ and $2a_{1g}$.

Lievens and co-workers [175] reported the first example of aromatic bimetallic cluster involving only σ orbitals, thus exhibiting σ-aromaticity. Using photofragmentation experiments they found that $[Au_5X]^+$ (X = V, Cr, Mn, Fe, Co) clusters show an anomalously high stability in mass abundance spectra [176]. In particular, quantum chemical calculations on the bimetallic $[Au_5Zn]^+$ cluster revealed that the cluster adopts a planar configuration with six σ valence electrons, thus satisfying the $(4n+2)$ electron-counting rule of σ aromaticity. The NICS values obtained at various positions inside, above or outside the molecular frame proved the existence of diatropic ring-current effect, characteristic for aromaticity. In a subsequent paper Lievens and co-workers [177] reported on 2D "magic" numbers in mass abundances of the photofragmented bimetallic $[Au_5X]^+$ (X = V, Cr, Mn, Fe, Co) clusters. They interpreted the enhanced stability of these particular doped gold clusters within a shell model approach for 2D systems. The six delocalized electrons in the 2D clusters corresponds to a "magic" number for electrons in a 2D box, which is also present in other 2D quantum systems such as semiconductor quantum dots. However, this "magic" number of electrons is compatible with the Hückel electron-counting rule of aromaticity. Interestingly, the main features of the molecular orbitals of the doped clusters were reproduced using a simple electron-in-a-box model.

The recent discovery of the extremely stable closed-shell bimetallic icosahedral gold clusters $W@Au_{12}$ and $Mo@Au_{12}$ by Wang and co-workers [178], first predicted by Pyykkö and Runeberg [179] opened up the field to new nano-sized gold materials, in which the central atom "impurity" plays a vital role in fine-tuning electronic properties. More recently [180], spectroscopic data (IR, Raman, UV–vis, Mössbauer and NMR) of $W@Au_{12}$ have been computed using DFT computational techniques. Population analysis revealed that the charge distribution is strongly delocalized but bonding regions are clearly seen. An isosurface of the electron-localization function (ELF) on a cut plane shown in Fig. 9 indicates the covalent part of the W–Au bond characterized by a local density maximum which seems to be pushed to the outer part of the cluster, leading to the peculiar shape of the Au atoms.

Most recently, Zhai et al. [181] reported the observation and characterization of a series of stable bimetallic clusters containing a highly symmetric 12-atom icosahedral Au cage with an encapsulated central heteroatom formulated as $[M@Au_{12}]^-$ (M = V, Nb, and Ta). These species adopting structures of high symmetry (icosahedral), exhibit remarkably high binding energies and stability indicative of spherical aromaticity.

The free-standing icosahedral cluster $[Pt@Pb_{12}]^{2-}$, that contains a Pt atom centered in a *closo*-$[Pb_{12}]^{2-}$ icosahedral Zintl ion was prepared and has been characterized by energy dispersive X-ray (EDX) analysis, ^{207}Pb and ^{195}Pt

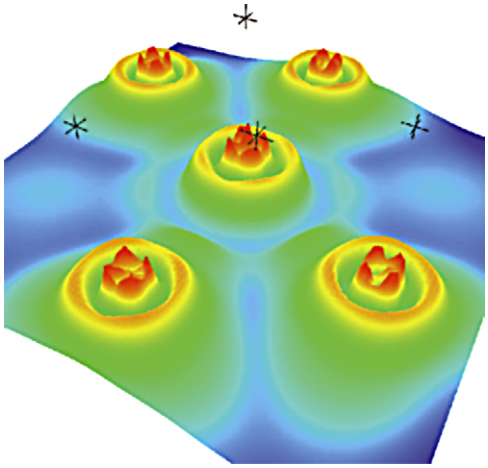

Fig. 9. Cut plane through the ELF of WAu_{12} [180]. Reproduced by permission of the PCCP Owner Societies.

NMR spectroscopy and single crystal XRD [182]. The $[Pt@Pb_{12}]^{2-}$ cluster is defined by an icosahedron of twelve Pb atoms with a centered Pt atom and has near-perfect I_h symmetry. It is a 12-vertex 26-electron polyhedron with a highly-regular *closo* icosahedral structure which follow Wade's $2n+2$ skeletal electron rule. The high stability of the $[Pt@Pb_{12}]^{2-}$ cluster could be attributed to spherical aromaticity characteristic of the closely related icosahedral aromatic $[Al@Pb_{10}]^+$ and $[Al@Pb_{12}]^+$ clusters [183]. The magic electronic character for the experimentally observed extremely stable metal-encapsulated $[Al@Pb_{10}]^+$ and $[Al@Pb_{12}]^+$ clusters was confirmed by the NICS(0) values, revealing their aromatic character (−26 and −20 ppm for the $[Al@Pb_{10}]^+$ and $[Al@Pb_{12}]^+$ clusters, respectively). Moreover, the observed stability of the $[Al@Pb_{10}]^+$ and $[Al@Pb_{12}]^+$ clusters reflected on the prominent abundances in the mass spectra and the large HOMO–LUMO gaps were attributed to the combined effect of highly symmetric close-packed structures, closed crystal-field split electron shell configurations, and a 3D aromatic character. Abundant binary alloy cluster anions were produced by laser ablation of mixtures of cobalt plus group-14 elements (E) [184]. The heteroclustering ability between Co and E elements increases from Ge to Pb, and the chemical bonds in the anionic binary alloy clusters might indicate a transition from covalent to metallic bonds. The cluster anion $[Co@Pb_{10}]^-$ appearing in very high abundance (magic number) adopts an endohedral structure, while the anionic $[Co@Pb_{12}]^-$ cluster also representing a magic number adopts probably an icosahedral structure. Metal-encapsulated icosahedral superatoms of germanium and tin formulated as $[Zn@Ge_{12}]$ and $[Cd@Sn_{12}]$ were predicted using ab initio pseudopotential plane wave and generalized gradient DFT computational techniques [185]. These clusters exhibit perfect icosahedral symmetry and large HOMO–LUMO gap lying in the optical region (about 2 eV), thus making these species attractive for self-assembled opto-electronic materials.

6.2. Ligand-stabilized all-metal $[M_nL_m]$ aromatic molecules

Experimental evidences for certain discrete trinuclear metal cluster compounds with $[M_3(\mu_3\text{-}X)(\mu\text{-}Y)_3]^{4+}$ (M = Mo, W; X, Y = O, S, Se, Te) cores containing puckered $\{M_3(\mu\text{-}Y)_3\}$ six-membered rings revealed benzene-like structural, magnetic and spectroscopic characteristics as well as chemical reactivities in a series of ligand substitution, addition, and oxidation reactions [45]. Based on an energy-localized analysis (LMO) the $[M_3(\mu_3\text{-}X)(\mu\text{-}Y)_3]^{4+}$ compounds were found to exhibit, like benzene, aromatic character due to a closed, completely continuous conjugated π-electron system, formed from the three cooperating 3c–2e π bonds, which are of the d-p-d type. The size and electronegativity of the bridging Y ligand affects significantly the degree of *quasi*-aromaticity of the puckered $\{M_3(\mu\text{-}Y)_3\}$ ring. Some criteria for the formation of a closed, smoothly continuous conjugated π-electron system in the $\{M_3(\mu\text{-}Y)_3\}$ rings have also been suggested. On the basis of the localized molecular orbital theory Chen [46] pointed out the multicentered bonding and *quasi*-aromaticity in metal-chalcogenide clusters. The bonding and electronic structures of 12 homo- and hetero-metallic trinuclear incomplete cubane-type aqua ions of transition metal clusters formulated as $[Mo_{3-n}W_nX_4(H_2O)_9]^{4+}$ (X = O, S, Se, Te; n = 0–3) have been investigated at the canonical molecular orbital (CMO) and LMO levels of theory [44]. It was found that the CMO distributions (Fig. 10) and the energy levels in these puckered $\{M_3X_3\}$ six-membered rings resemble those of benzene. According to the LMO analysis (Fig. 11) these molecules exhibit *quasi*-aromaticity, which is related to a set of three continuous and closed 3c–2e (d-p-d) π bonds with strong interactions.

A combined matrix isolation Fourier transform infrared (FTIR) spectroscopic and theoretical study (B3LYP/6-311+G*, CCSD(T)/6-31+G* and single point G3, G3S, G3SCB, and CCSD(T)/6-31+G(2-Df)) on the $Al_2(CO)_2$ molecule has been reported recently [186]. The $Al_2(CO)_2$ molecule was predicted to be aromatic based on structural, energetic, and magnetic criteria. The HOMO ($3b_{3u}$) of $Al_2(CO)_2$ in its singlet ground state is a completely delocalized p_π orbital of the Al_2C_2 unit, and having two π electrons satisfies the $4n+2$ electron-counting rule for aromatic compounds. The digallium dicarbonyl, $Ga_2(CO)_2$ produced and identified in thermal gallium atom reactions with CO in solid argon [187] exhibits the same bonding properties with the dialuminum dicarbonyl. Both species have about the same NICS(0) values of −16.70 and −20.14 ppm, respectively and constitute the first neutral heterocyclic all-metal aromatic molecules.

The structures of In_NO (N = 1–8) clusters, produced using a laser vaporization cluster source, laser ionized and mass selectively recorded by a time-of-flying mass spectrometer, were computed employing DFT at the B3LYP level of theory [188]. The bonding in these clusters was analyzed by means of Bader's atoms in molecules (AIM) method. Exceptionally

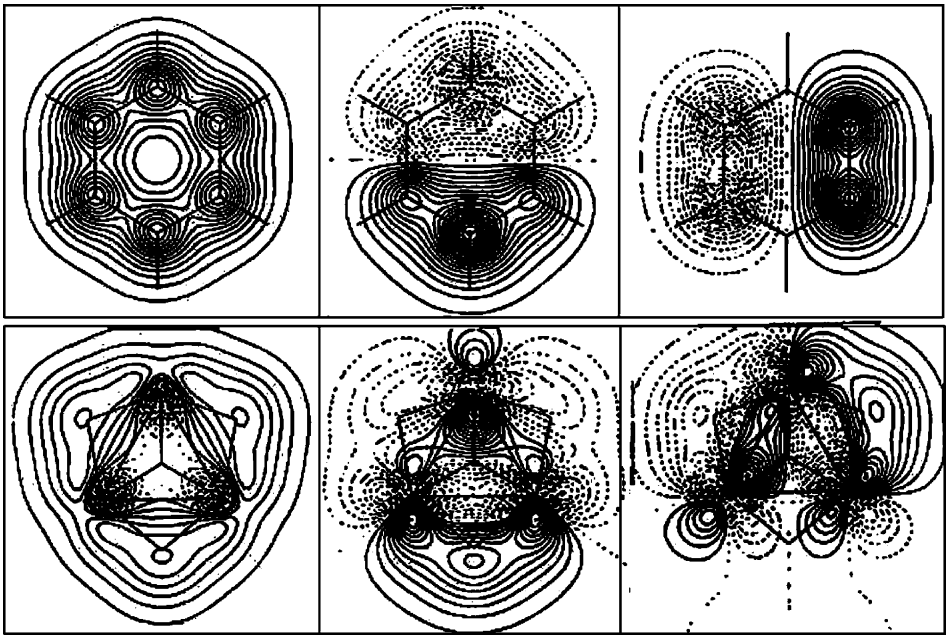

Fig. 10. (a) (p-p) π bonding CMOs ($a_{2g} + e_{1g}$) in C_6H_6, (b) (d-p) π bonding CMOs ($a_1 + e$) in $Mo_3(\mu\text{-}S_b)_3$. Reproduced with permission from [44]. Copyright by Springer Science and Business Media.

low ionization potentials were obtained for In_3O and In_7O clusters. Ionization of these clusters yields the highly symmetric cationic $[In_3O]^+$ and $[In_7O]^+$ clusters. The magnetic properties of the $[In_7O]^+$ cluster suggest its "magic number" character, with 18 delocalized electrons. Notice that valence electrons behave as if they were nearly free in clusters when the number of such itinerant electrons corresponds to a spherical shell closure. The computed GIAO NMR chemical shifts for the $[In_7O]^+$ cluster indicated that not only the shielding of the O atom is exceptionally positive, but also the In shieldings are the largest among all the clusters studied. Based on the magnetic shielding criteria of aromaticity the $[In_7O]^+$ cluster possesses aromatic character. On the other hand, the $[In_3O]^+$ cluster does not indicate a "magic number" character.

Very recently novel ligand stabilized clusters of elements of group 14 exhibiting trishomoaromaticity have been syn-

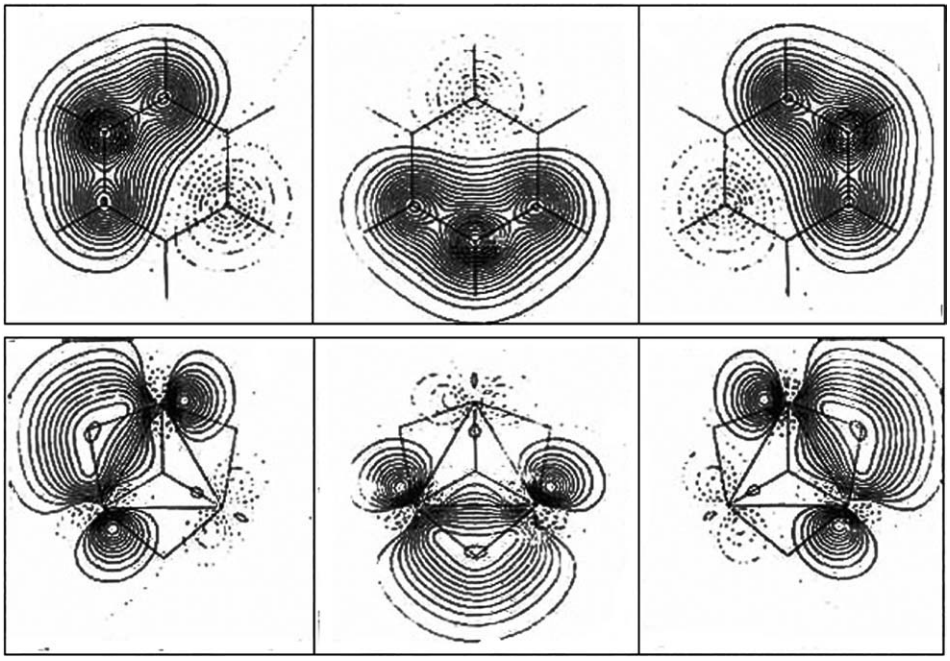

Fig. 11. (a) (p-p-p) π 3c–2e LMOs in C_6H_6, (b) (d-p-d) π 3c–2e LMOs in $Mo_3(\mu\text{-}S_b)_3$. Reproduced with permission from [44]. Copyright by Springer Science and Business Media.

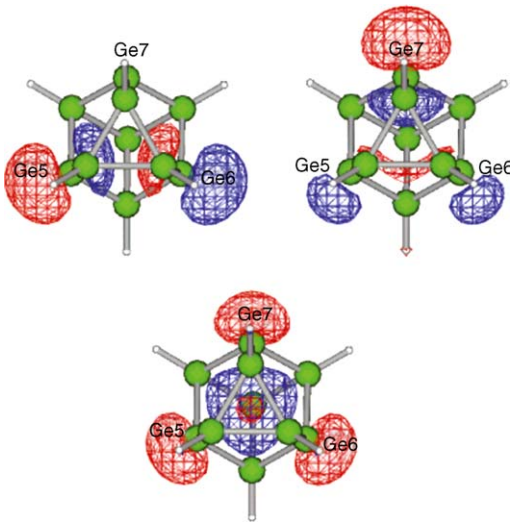

Fig. 12. HOMO (below) and two degenerate LUMOs (upper) for $[Ge_{10}H_7]^+$ at MP2/6-31G(d)//B3LYP/6-31G(d). Reproduced with permission from [189]. Copyright by the Wiley-VCH Verlag GmbH&Co. KgaA, Weinheim.

thesized and studied both experimentally and theoretically [189,190]. Sekiguchi et al. [191–193] synthesized and characterized the long-sought free cyclotrigermenylium cation $[(^tBu_3Si)_3Ge_3]^+$, **11** with a Ge_3 equilateral triangle which is an aromatic 2π-electron system analogous to cyclopropenium cation $[C_3R_3]^+$. More recently [189] they have also synthesized the cationic cluster compound $[Ge_{10}(^tBu_3Si)_6I]^+$, **12** containing three naked germanium atoms.

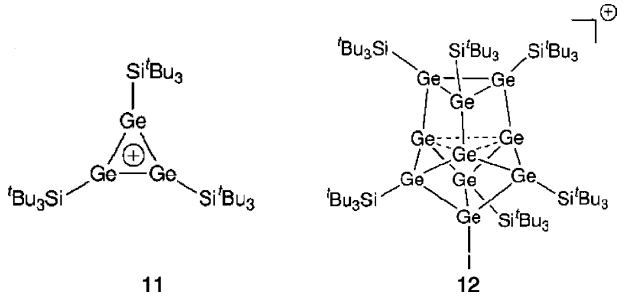

11 12

DFT calculations at the B3LYP/6-31G(d) level on the model compound $[Ge_{10}H_7]^+$, **13** with C_{3v} symmetry revealed the same cluster skeleton as a global minimum. The HOMO of **13** (Fig. 12) indicates the presence of bonding interactions between the Ge atoms in the three-membered ring forming a 3c–2e bond by charge density delocalization inside the conjugative central core being characteristic of aromaticity. The aromatic character of **13** was further substantiated by evaluation of the aromatic stabilization energy (ASE) (−19.2 kcal/mol) and the strongly diatropic NICS(0) value of −24.6 ppm.

Aromaticity has been also identified in binary and ternary semiconductor systems with three- or four-membered planar rings using electronic structure calculation methods at the MP2 and DFT levels of theory [194,195]. The highly strained ring systems $[A_3R_3]^+$, $[A_2BR_3]^+$, $[GeSiCr_3]^+$, $[A_3R_3Ha]$, and $[A_4R_4]^{2+}$ (A, B = C, Si, Ge; R–H, SiH_3; Ha = F, Cl, Br) are confirmed to be featured with delocalized π orbitals perpendicular to the molecular planes and have high negative NICS(0) values in the range of –15 to –22 ppm. All semiconductor species exhibit characteristics of delocalized 2-electron π orbitals and therefore are aromatic systems. The same holds true for the carbon-rich binary and ternary semiconductor microclusters $Ge_lSi_mC_n$ ($7 \le s = l + m + n \le 10$ with $n = 5$–8) studied by Li et al. using DFT and MP2 computational techniques. It was predicted that the singly or doubly charged $Ge_lSi_mC_nH_x$ species conforming to the $(4n + 2)$π-electron-counting rule possess aromatic character depending on the delocalized π bonds sustained by the closed cyclic molecular skeletons.

The presence of aromaticity was also recognized in organometallic compounds involving all-metal ring cores. Very recently King [59] introduced the σ-aromaticity concept to describe the bonding in triangular metal carbonyl clusters, $M_3(CO)_{12}$ (M = Fe, Ru, Os). According to this model the six orbitals and six electrons available for bonding within the M_3 triangle of $M_3(CO)_{12}$ clusters are partitioned into a core 3c–2e bond of Hückel topology formed by radial hybrid orbitals and a surface 3c–4e bond of Möbius topology formed by tangential p-orbitals. The σ-aromaticity concept has also been applied to the description of the bonding in planar triangular $Pt_3(CO)_3(\mu\text{-}CO)_3$ building blocks of platinum carbonyl structures including the $[Pt(CO)_2]_n^{2-}$ stacks. Notice that the presence of the bridging CO ligands in $Pt_3(CO)_3(\mu\text{-}CO)_3$ cluster precludes the 3c–4e Möbius topology. The σ-aromaticity model for the bonding in metal carbonyl triangles contains many of the features of the graph-theory model for the 3D aromaticity in deltahedral structures.

King has also studied the chemical bonding topology of ternary transition metal-centered bismuth cluster halides [196]. Examples of neutral or ionic transition metal-centered bismuth clusters are octahedral $[MBi_6(\mu\text{-}X)_{12}]^{z-}$ (X = Br, I; M = Rh, Ir, z = 3; M = Ru, z = 4) with exclusive 2c–2e bonds and pentagonal bipyramidal $RhBi_7Br_8$ with a 5d–4e bond in the equatorial plane suggestive of Möbius aromaticity (Fig. 13).

The chemical bonding in many of the ternary transition metal-centered bismuth cluster halides is related to that of the

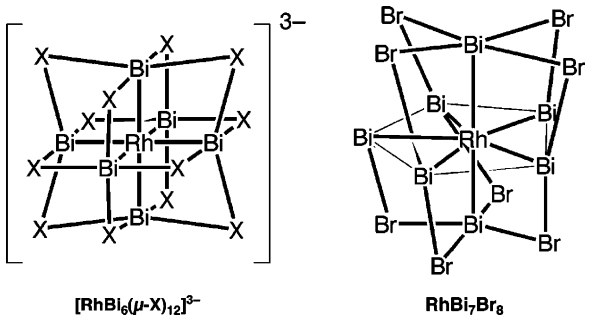

Fig. 13. Structures of $[RhBi_6(\mu\text{-}X)_{12}]^+$ (X = Br, I) ions and the $RhBi_7Br_8$ molecule. Reproduced with permission from [196]. Copyright by the American Chemical Society.

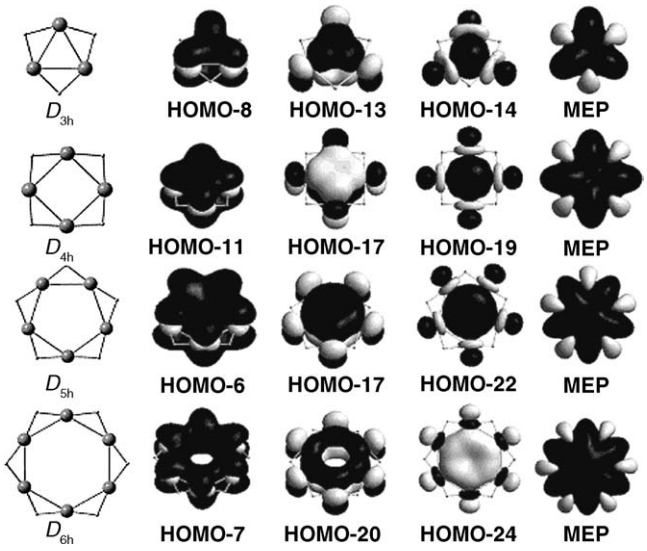

Fig. 14. Selected highly delocalized molecular orbitals along with the molecular electrostatic potential (MEP) of the planar cyclic Cu_nH_n molecules contributing to aromaticity. Reproduced with permission from [197]. Copyright by the American Chemical Society.

deltahedral boranes exhibiting 3D aromaticity by replacing the multicenter core bond in the boranes with 2c–2e bonds from the central transition metal to the bismuth atom. The electron counts of the $RuBi_5$, $RuBi_8$ and Ru_2Bi_4 polyhedral structural units follow the Wade-Mingos rules.

6.3. Hydrometal analogues of aromatic hydrocarbons

The possibility for hydrometal analogues of the aromatic hydrocarbons has been explored very recently [197,198]. Quantum chemical calculations suggested that a series of molecules with the general formula *cyclo*-$M_n(\mu\text{-}H)_n$ (M = Cu, Ag, Au; n = 3–6) are stable. All *cyclo*-M_nH_n species, except *cyclo*-Au_3H_3, have the same symmetry with the respective aromatic hydrocarbons, but differ in that the hydrogen atoms are in bridging positions between the metal atoms and not in terminal positions. These novel classes of inorganic compounds can be considered as the archetypes for the development of whole classes of new inorganic aromatic species (substituted derivatives) resulting upon substitution of the H atoms by other groups, such as alkyls (R) and aryls (Ar), halides (X), amido (NR_2), hydroxide (OH) and alkoxides (OR), etc. Novel low-energy 3D structures of the Cu_nH_n, Ag_nH_n and Au_nH_n (n = 3–6) molecules were also identified as local minima in the potential energy surfaces, but at 27–59 kcal/mol higher in energy than the 2D planar ones. The planar hydrocoppers(I), hydrosilvers(I) and hydrogolds(I) are predicted to be strongly bound molecules with respect to their dissociation either to the MH monomers or to free M and H atoms in their ground states. The computed total binding energies of the MH monomers to form the *cyclo*-M_nH_n species are found in the range of 7.5–217.5 kcal/mol.

The bonding of all *cyclo*-$M_n(\mu\text{-}H)_n$ species is characterized by a common ring-shaped electron density, more commonly seen in organic molecules, which is constructed by highly delocalized σ-, π- and δ-type MOs (Fig. 14).

The aromaticity of the hydrocopper(I), hydrosilver(I) and hydrogold(I) analogues of aromatic hydrocarbons was estimated by making use of several criteria for aromaticity, such as the NICS(0) parameter, the relative hardness $\Delta\eta$ and the electrophilicity index ω. It was further verified on the grounds of a chemical reactivity criterion of aromaticity that of the interaction of the aromatics with electrophiles, presenting only one example concerning the reaction of *cyclo*-$Au_6(\mu\text{-}H)_6$ molecule with Ag^+ ions. Actually, this interaction affords the $[Ag\{cyclo\text{-}Au_6(\mu\text{-}H)_6\}]^+$ species, **14**, which adopts an hexagonal pyramidal structure of C_{6v} symmetry with the silver(I) ion displaced along the C_6 axis over the hexagonal basal plane by 91.8 pm [198].

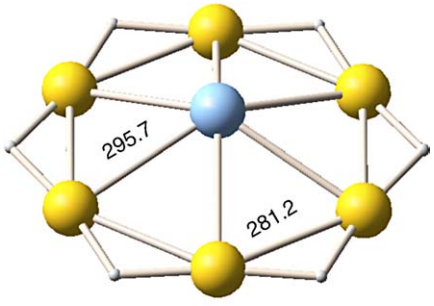

14

The bonding of the central Ag(I) ion with the six-membered gold(I) ring involves covalent σ, π and δ components as it is exemplified by the highly delocalized σ-, π- and δ-type MOs, which support a charge transfer from the six Au(I) atoms towards the Ag(I) central atom, the latter acquiring a positive natural charge of 0.56 charge units. This charge transfer is also mirrored on the deshielding of the Au(I) atoms, which showed a downfield shift of the ^{197}Au shielding tensor element by 15.7 ppm. Moreover, the computed interaction energy between the Ag(I) ion and the aromatic six-membered gold(I) ring was found to be 52.1 kcal/mol and corresponds to 8.7 kcal/mol per Ag–Au bond, a value lying in the range of the so-called aurophilic interaction energy[198].

The proposal of aromatic hydrocopper Cu_4H_4 and Cu_5H_5 stimulated Li et al. [199,200] to explore by means of DFT computational techniques planar tetracoordinated and pentacoordinated nonmetals hosted on perfect square planar and pentagonal hydrocopper complexes Cu_4H_4X and Cu_5H_5X (X = B, C, N, O), respectively. The bonding in these complexes has been analyzed using molecular orbital and natural bond orbital analysis techniques. It was found that the X atoms serve as the negatively charged nonmetal centers, and the Cu atoms at the periphery form a positively charged ring. The optimized structures of D_{5h} Cu_5H_5X complexes and their HOMOs are shown in Fig. 15.

It was also found that the introduction of X at the center of the aromatic hydrocopper(I) rings vanishes the aromatic character and therefore the doped rings are nonaromatic.

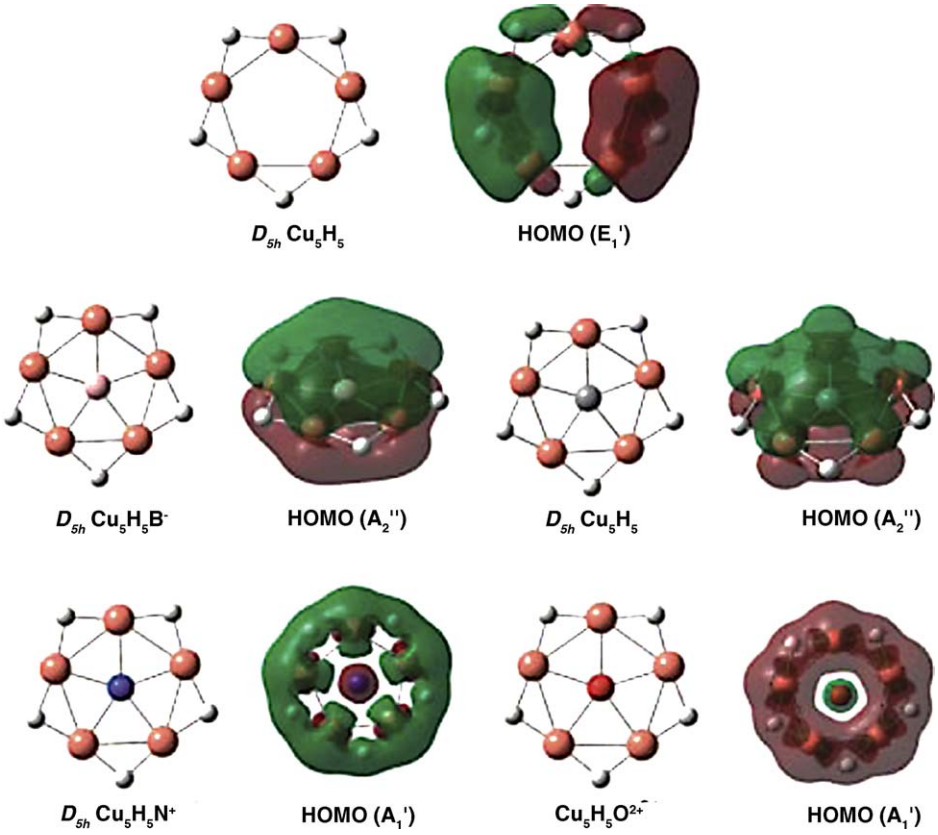

Fig. 15. Optimized structures of D_{5h} Cu_5H_5X complexes (X = B, C, N, O) and their HOMO diagrams compared with that of hydrocopper D_{5h} Cu_5H_5 at the B3LYP/6-311+G(3df, p) level. Reproduced with permission from [200]. Copyright by the Wiley-VCH Verlag GmbH, Weinheim.

However, this finding seems to be questionable, since assessment of the aromaticity was based only on the up-field chemical shifts of the H atoms outside the metallic ring. Probably the chemical shift of the central atom X might be more informative for aromaticity of the Cu_nH_nX molecules.

7. Conclusions and perspectives

In this review I have tried to summarize the current state of research related to all-metal aromatic molecules. I have deliberately devoted considerable attention on the discussion of the DFT methods, since they have contributed much in the study of all-metal aromatic systems by predicting their structural, energetic, electronic and spectroscopic properties and demonstrating the extensive cyclic delocalization of electron density in these systems. The recent advances in the field of quantum inorganic chemistry bold great promise for the future discovery of new series of novel aromatic metal clusters and transition metal coordination compounds and organometallics with particular properties and functionality, guiding experimentalists to synthesize them. A daunting challenge for the future is to explore the physical, chemical, biological, and technical properties of such molecules, and to look for their technical applications as specific and very efficient catalysts, drugs, and other novel materials with as-yet unimagined properties.

The traditional indicators of aromaticity – structural, magnetic, energetic, electronic and reactivity-based criteria – used to study the aromaticity in all-metal aromatic molecules, many of which are accessible through quantum chemical calculations were also outlined herein. All-metal aromatic molecules represent one of the “new frontiers” that promise to keep aromatic chemistry vibrant well into the 21st century. It is expected that understanding the origin of aromaticity in all-metal systems would further widen the view at aromaticity illustrating its multidimensional character and helping us deeper understand what other factors govern structural patterns and stability of solids.

References

[1] A. Kekulé, Bull. Soc. Chim. Fr. 3 (1866) 98.
[2] A. Kekulé, Bull. Acad. R. Belg. 19 (1965) 551.
[3] A. Kekulé, Z. Chem. (Neue Folge) 1 (1965) 277.
[4] A. Kekulé, Ann. Chem. Pharm. 137 (1865) 129.
[5] A. Kekulé, Liebigs Ann. Chem. 137 (1866) 1866.
[6] A. Kekulé, Ber. Dtsch. Chem. Ges. 2 (1869) 362.
[7] A. Kekulé, Lehrbuch der organischen chemie, Verlag Ferdinand Enke, Erlangen II, 1866.

[8] E. Hückel, Z. Phys. 70 (1931) 204.
[9] F. De Proft, P. Geerlings, Phys. Chem. Chem. Phys. 6 (2004) 242.
[10] P.C. Hiberty, S. Shaik, Phys. Chem. Chem. Phys. 6 (2004) 224.
[11] P. Lazzeretti, Phys. Chem. Chem. Phys. 6 (2004) 217.
[12] T.M. Krygowski, M.K. Cyrański, Phys. Chem. Chem. Phys. 6 (2004) 249.
[13] E. Steiner, P.W. Fowler, Phys. Chem. Chem. Phys. 6 (2004) 261.
[14] C. Corminboeuf, T. Heine, G. Seifert, P.v.R. Schleyer, J. Weber, Phys. Chem. Chem. Phys. 6 (2004) 273.
[15] A. Rasat, Phys. Chem. Chem. Phys. 6 (2004) 232.
[16] R.W.A. Havenith, P.W. Fowler, E. Steiner, S. Shetty, D. Kanhere, S. Pal, Phys. Chem. Chem. Phys. 6 (2004) 285.
[17] R.W.A. Havenith, J.J. Engelberts, P.W. Fowler, E. Steiner, J.H. van Lenthe, P. Lazzeretti, Phys. Chem. Chem. Phys. 6 (2004) 289.
[18] B. Silvi, Phys. Chem. Chem. Phys. 6 (2004) 256.
[19] R.B. King, Chem. Rev. 101 (2001) 1119.
[20] M. Bühl, A. Hirsch, Chem. Rev. 101 (2001) 1153.
[21] R.W. Williams, Chem. Rev. 101 (2001) 1185.
[22] J.R. Bleeke, Chem. Rev. 101 (2001) 1205.
[23] L. Nyulászi, Chem. Rev. 101 (2001) 1229.
[24] V.I. Minkin, R.M. Minyaev, Chem. Rev. 101 (2001) 1247.
[25] M.D. Watson, A. Fechtenkötter, K. Müllen, Chem. Rev. 101 (2001) 1267.
[26] K.B. Wiberg, Chem. Rev. 101 (2001) 1317.
[27] J.A.N.F. Gomes, R.B. Mallion, Chem. Rev. 101 (2001) 1349.
[28] T.M. Krygowski, M.K. Cyrański, Chem. Rev. 101 (2001) 1385.
[29] A.R. Katritzky, K. Jug, D.C. Oniciu, Chem. Rev. 101 (2001) 1421.
[30] R.H. Mitchell, Chem. Rev. 101 (2001) 1301.
[31] S. Shaik, A. Shurki, D. Danovich, P.C. Hiberty, Chem. Rev. 101 (2001) 1501.
[32] L.J. Schaad, B.A.J. Hess, Chem. Rev. 101 (2001).
[33] F. De Proft, P. Geerlings, Chem. Rev. 101 (2001) 1451.
[34] S.W. Slayden, J.F. Liebman, Chem. Rev. 101 (2001) 1541.
[35] V.I. Minkin, M.N. Glukhovtsev, B.Y. Simkin, Aromaticity and Antiaromaticity: Electronic and Structural Aspects, J. Wiley & Sons, New York, 1994.
[36] T.M. Krygowski, M.K. Cyrański, Z. Czarnocki, G. Hafelinger, A.R. Katritzky, Tetrahedron 56 (2000) 1783.
[37] P.v.R. Schleyer, H. Jiao, N.v.E. Hommes, V.G. Malkin, O.L. Malkina, J. Am. Chem. Soc. 119 (1997) 12669.
[38] C.W. Bird, Tetrahedron 54 (1998) 4641.
[39] B. Goldfuss, P.v.R. Schleyer, Organometallics 16 (1997) 1543.
[40] R.B. King, J. Chem. Inf. Comput. Sci. 32 (1992) 42.
[41] A. Hirsch, Z. Chen, H. Jiao, Angew. Chem., Int. Ed. 40 (2001) 2834.
[42] R.B. King, J. Chem. Inf. Comput. Sci. 41 (2001) 517.
[43] S. Winstein, J. Am. Chem. Soc. 81 (1959) 6524.
[44] J. Li, C.-W. Liu, J.-X. Lu, J. Clust. Chem. 7 (1996) 469.
[45] J.-X. Lu, Z.-D. Chen, Int. Rev. Phys. Chem. 13 (1994) 85.
[46] Z. Chen, J. Clust. Chem. 6 (1995) 357.
[47] A.R. Katritzky, M. Karelson, A.P. Wells, J. Org. Chem. 61 (1996) 1619.
[48] A.R. Katritzky, P. Barczynski, G. Musumarra, D. Pisano, M. Szafran, J. Am. Chem. Soc. 111 (1989) 7.
[49] A.R. Katritzky, V. Feygelman, G. Musumarra, P. Barczynski, M. Szafran, J. Prakt. Chem./Chem. Ztg. 332 (1990) 853.
[50] A.R. Katritzky, M. Karelson, N. Malhotra, Heterocycles 32 (1991) 127.
[51] E. Heilbronner, Tetrahedron Lett. (1964) 1923.
[52] T. Kawase, M. Oda, Angew. Chem., Int. Ed. 43 (2004) 2.
[53] M.J.S. Dewar, J. Am. Chem. Soc. 106 (1984) 669.
[54] M.J.S. Dewar, R. Pettit, J. Chem. Soc. (1954) 1625.
[55] M.J.S. Dewar, Bull. Soc. Chim. Belg. 88 (1979) 957.
[56] M.J.S. Dewar, M.L. NMcKee, Pure Appl. Chem. 52 (1980) 1431.
[57] K. Exner, P.v.R. Schleyer, J. Phys. Chem. A 105 (2001) 3407.
[58] D. Cremer, Tetrahedron 44 (1988) 7427.
[59] R.B. King, Inorg. Chim. Acta 350 (2003) 126.
[60] M.J.S. Dewar, Angew. Chem., Int. Ed. Engl. 10 (1971) 761.
[61] O.E. Polansky, G. Derflinger, Int. J. Quantum Chem. 1 (1967) 379.
[62] M.K. Bremer, Chem. Eng. News Dec 20 (1999).
[63] Z. Chen, H. Jiao, A. Hirsch, P.v.R. Schleyer, Angew. Chem., Int. Ed. 41 (2002) 4309.
[64] M. Reiher, A. Hirsch, Chem. Eur. J. 9 (2003) 5442.
[65] W.A. De Heer, Rev. Mod. Phys. 65 (1993) 611.
[66] M. Brack, Rev. Mod. Phys. 65 (1993) 677.
[67] C. Yannouleas, U. Landman, Phys. Rev. B 51 (1995) 1902.
[68] J. Poater, X. Fradera, M. Duran, M. Solá, Chem. Eur. J. 9 (2003) 400.
[69] P.v.R. Schleyer, H. Jiao, Pure Appl. Chem. 68 (1996) 209.
[70] M.N. Glukhovtsev, P.v.R. Schleyer, Chem. Phys. Lett. 198 (1992) 547.
[71] C.H. Suresh, N. Koga, J. Org. Chem. 67 (2002) 1965.
[72] P. George, M. Trachtman, C.W. Bock, A.M. Brett, J. Chem. Soc., Perkin Trans. 2 (1977) 1036.
[73] D.L. Cooper, J. Gerratt, M. Raimondi, Chem. Rev. 91 (1991) 929.
[74] D.L. Cooper, J. Gerratt, M. Raimondi, Top. Curr. Chem. 153 (1990) 41.
[75] J. Gerratt, D.L. Cooper, P.B. Karakakov, M. Raimondi, Chem. Soc. Rev. 26 (1997) 87.
[76] P.v.R. Schleyer, F. Puhlhofer, Org. Lett. 4 (2002) 2873.
[77] T.M. Krygowski, J. Chem. Inf. Comp. Sci. 33 (1993) 70.
[78] J. Kruszewski, T.M. Krygowski, Tetrahedron Lett. (1972) 3839.
[79] D.H. Hutter, W.H. Flygare, Top. Curr. Chem. 63 (1976) 89, and references therein.
[80] W.H. Flygare, Chem. Rev. 74 (1974) 653.
[81] H.J. Dauben Jr., J.D. Wilson, J.L. Laity, J. Am. Chem. Soc. 90 (1968) 811.
[82] P. Lazzeretti, in: J.W. Emsley, J. Feeney, L.H. Sutcliffe (Eds.), Progress in Nuclear Magnetic Resonance Spectroscopy, Elsevier, Amsterdam, 2000, pp. 1–88.
[83] C.W. Haigh, R.B. Mallion, Croat. Chem. Acta 62 (1989) 1.
[84] T.A. Keith, R.F.W. Bader, J. Chem. Phys. 99 (1993) 3669.
[85] P. Lazzeretti, M. Malagoli, R. Zanasi, Chem. Phys. Lett. 220 (1994) 299.
[86] S. Coriani, P. Lazzeretti, M. Malagoli, R. Zanasi, Theor. Chim. Acta 89 (1994) 181.
[87] R. Zanasi, P. Lazzeretti, M. Malagoli, F. Piccinini, J. Chem. Phys. 102 (1995) 7150.
[88] P. Lazzeretti, R. Zanasi, Int. J. Quantum Chem. 60 (1996) 249.
[89] A. Keith, R.F.W. Bader, Chem. Phys. Lett. 210 (1993) 223.
[90] R.W.A. Havenith, A. Rassat, P.W. Fowler, J. Chem. Soc., Perkin Trans. 2 723 (2002) 2002.
[91] E. Steiner, P.W. Fowler, J. Phys. Chem. A 105 (2001) 9553.
[92] E. Steiner, P.W. Fowler, J. Chem. Soc., Chem. Commun. (2001) 2220.
[93] G. Merino, T. Heine, G. Seifert, Chem. Eur. J. 10 (2004) 4367.
[94] P.v.R. Schleyer, C. Maerker, A. Dransfeld, H. Jiao, N.J.R. van Eikema Hommes, J. Am. Chem. Soc. 118 (1996) 6317.
[95] P.v.R. Schleyer, M. Manoharan, Z. Wang, X.B. Kiran, H. Jiao, R. Puchta, N.J. Eikema Hommes, Org. Lett. 3 (2001) 2465.
[96] P.v.R. Schleyer, H. Jiao, N.J. Eikema Hommes, V.G. Malkin, O.L. Malkina, J. Am. Chem. Soc. 119 (1997) 12669.
[97] T. Heine, P.v.R. Schleyer, C. Corminboeuf, G. Seifert, R. Reviakine, J. Weber, J. Phys. Chem. A 107 (2003) 6470.
[98] S. Klod, E. Kleinpeter, J. Chem. Soc., Perkin Trans. 2 (2001) 1893.
[99] S. Klod, A. Koch, E. Kleinpeter, J. Chem. Soc., Perkin Trans. 2 (2002) 1506.
[100] D. Amic, N. Trinajsitc, Bull. Soc. Chim. Belg. 100 (1991) 527.
[101] R. Contreras, V.S. Safont, P. Peréz, J. Andres, V. Moliner, O. Tapia, J. Mol. Struct. (THEOCHEM) 426 (1998) 277.
[102] C. Lepetit, M.B. Nielsen, F. Diederich, R. Chauvin, Chem. Eur. J. 9 (2003) 5056.
[103] G.P. Bean, J. Org. Chem. 63 (1998) 2497.
[104] N. Sadlej-Sosnowska, J. Org. Chem. 66 (2001) 8737.

[105] R.F.W. Bader, Acc. Chem. Res. 18 (1985) 9.
[106] R.F.W. Bader, Chem. Rev. 91 (1991) 893.
[107] R.F.W. Bader, Atoms in Molecules: A Quantum Theory, Oxford, 1990.
[108] S.T. Howard, T.M. Krygowski, Can. J. Chem. 75 (1997) 1174.
[109] R.G. Pearson, Chemical Hardness, Wiley, New York, 1997.
[110] C.H. Sursesh, S.R. Gadre, J. Org. Chem. 64 (1999) 2505.
[111] D.B. Chesnut, L. Bartolotti, J. Chem. Phys. 253 (2000) 1.
[112] X. Fradera, M.A. Austen, R.F.W. Bader, J. Phys. Chem. A 103 (1999) 304.
[113] D.B. Chesnut, L.J. Bartolotti, Chem. Phys. 257 (2000) 175.
[114] J. Poater, M. Solá, M. Duran, X. Fradera, J. Phys. Chem. A 105 (2001) 2052.
[115] J. Poater, M. Solá, M. Duran, X. Fradera, J. Phys. Chem. A 106 (2002) 4794.
[116] X. Fradera, J. Poater, S. Simon, M. Duran, M. Solá, Theor. Chem. Acc. 108 (2002) 214.
[117] J. Poater, M. Solá, M. Duran, X. Fradera, J. Phys. Chem. A 105 (2001) 6249.
[118] S. Sakai, J. Phys. Chem. A 106 (2002) 10370.
[119] S. Sakai, J. Phys. Chem. A 106 (2002) 11526.
[120] S. Sakai, J. Phys. Chem. A 107 (2003) 9422.
[121] X.-W. Li, W.T. Pennington, G.H.A. Robinson, J. Am. Chem. Soc. 117 (1995) 7578.
[122] Y. Xie, P.R. Schreiner, H.F. Schaefer III, X.-W. Li, G.H. Robinson, J. Am. Chem. Soc. 118 (1996) 10635.
[123] G.H.A. Robinson, Acc. Chem. Res. 32 (1999) 773.
[124] X.-W. Li, Y. Xie, P.R. Schreiner, K.D. Gripper, R.C. Crittendon, C.F. Campana, H.F. Schaefer, G.H. Robinson, Organometallics 15 (1996) 3798.
[125] B. Twamley, P.P. Power, Angew. Chem., Int. Ed. 39 (2000) 3500.
[126] A.E. Kuznetsov, A.I. Boldyrev, X. Li, L.-S. Wang, J. Am. Chem. Soc. 123 (2001) 8825.
[127] X. Li, A.E. Kuznetsov, H.-F. Zhang, A.I. Boldyrev, L.-S. Wang, Science 291 (2001) 859.
[128] A.E. Kuznetsov, J.D. Corbet, L.-S. Wang, A.I. Boldyrev, Angew. Chem., Int. Ed. 40 (2001) 3369.
[129] X. Li, H.-F. Zhang, L.-S. Wang, A.E. Kuznetsov, N.A. Cannon, A.I. Boldyrev, Angew. Chem., Int. Ed. 40 (2001) 1867.
[130] A.I. Boldyrev, A.E. Kuznetsov, Inorg. Chem. 41 (2002) 532.
[131] A.E. Kuznetsov, A.I. Boldyrev, H.J. Zhai, X. Li, L.-S. Wang, J. Am. Chem. Soc. 124 (2002) 11791.
[132] A.E. Kuznetsov, A.I. Boldyrev, Struct. Chem. 13 (2002) 141.
[133] A.N. Alexandrova, A.I. Boldyrev, J. Phys. Chem. A 107 (2003) 554.
[134] A.I. Boldyrev, L.-S. Wang, J. Phys. Chem. A 105 (2001) 10759.
[135] D.M. Bishop, M. Chaillet, K. Larrieu, C. Pouchan, Mol. Phys. 51 (1984) 179.
[136] A.E. Kuznetsov, A.I. Boldyrev, Chem. Phys. Lett. 388 (2004) 452.
[137] P.H. Acioli, J. Jellinek, Phys. Rev. Lett. 89 (2002) 213402.
[138] Y. Zhao, S. Li, W.-G. Xu, Q.-S. Li, J. Phys. Chem. A 108 (2004) 4887.
[139] I.G. Kaplan, O. Dolgounitcheva, J.D. Watts, J.V. Ortiz, J. Chem. Phys. 117 (2002) 3687.
[140] C.-G. Zhan, F. Zheng, D.A. Dixon, J. Am. Chem. Soc. 124 (2002) 14795.
[141] R.W.A. Havenith, J.H. van Lenthe, Chem. Phys. Lett. 385 (2004) 198.
[142] P.W. Fowler, R.W.A. Havenith, E. Steiner, Chem. Phys. Lett. 342 (2001) 85.
[143] Z. Chen, C. Corminboeuf, T. Heine, J. Bohmann, P.v.R. Schleyer, J. Am. Chem. Soc. 125 (2003) 13930.
[144] S. Shetty, D.G. Kanhere, S. Pal, J. Phys. Chem. A 108 (2004) 628.
[145] A. Datta, S.K. Pati, J. Phys. Chem. A 108 (2004) 9527.
[146] J.M. Mercero, J.M. Ugalde, J. Am. Chem. Soc. 126 (2004) 3380.
[147] A.E. Kuznetsov, H.J. Zhai, L.-S. Wang, A.I. Boldyrev, Inorg. Chem. 41 (2002) 6062.
[148] H.J. Zhai, L.-S. Wang, A.E. Kuznetsov, A.I. Boldyrev, J. Phys. Chem. A 106 (2002) 5600.
[149] M. Lein, J. Frunzke, G. Frenking, Angew. Chem., Int. Ed. 42 (2003) 1303.
[150] J. Frunzke, M. Lein, G. Frenking, Organometallics 21 (2002) 3351.
[151] M. Lein, J. Frunzke, G. Frenking, Inorg. Chem. 42 (2003) 2504.
[152] G. Frenking, K. Wichmann, N. Frohlich, C. Loschen, M. Lein, J. Frunzke, V.M. Rayon, Coord. Chem. Rev. 238–239 (2003) 55.
[153] I. Todorov, S.C. Sevov, Inorg. Chem. 43 (2004) 6490.
[154] P. Schwerdtfeger, Angew. Chem., Int. Ed. 42 (2003) 1892, and references therein.
[155] H. Häkkinen, M. Moseler, U. Landman, Phys. Rev. Lett. 89 (2002) 033401.
[156] H. Häkkinen, B. Yoon, U. Landman, X. Li, H.J. Zhai, L.-S. Wang, J. Phys. Chem. A 107 (2003) 6168.
[157] H. Häkkinen, U. Landman, Phys. Rev. B 62 (2000) R2287.
[158] G. Bravo-Pérez, I.L. Garzón, O. Novaro, J. Mol. Struct. THEOCHEM 493 (1999) 225.
[159] V. Bonačić-Koutecký, J. Burda, R. Mitrić, M. Ge, G. Zampella, P. Fantucci, J. Chem. Phys. 117 (2002) 3120.
[160] S. Gilb, P. Weis, F. Furche, R. Ahlrichs, M.M. Kappes, J. Chem. Phys. 116 (2002) 4094.
[161] F. Furche, R. Ahlrichs, P. Weis, C. Jacob, S. Gilb, T. Bierweiler, M.M. Kappes, J. Chem. Phys. 117 (2002) 6982.
[162] H.M. Lee, M. Ge, B.R. Sahu, P. Tarakeshwar, K.S. Kim, J. Phys. Chem. B 107 (2003) 9994.
[163] E.M. Fernández, J.M. Soler, I.L. Garzón, L.C. Balbas, Phys. Rev. B 70 (2004) 165403.
[164] J. Wang, G. Wang, J. Zhao, Chem. Phys. Lett. 380 (2003) 716.
[165] J. Li, X. Li, H.J. Zhai, L.-S. Wang, Science 299 (2003) 864.
[166] R.B. King, Z. Chen, P.v.R. Schleyer, Inorg. Chem. 43 (2004) 4564.
[167] H.-F. Zhang, M. Stender, R. Zhang, G. Wang, J. Li, L.-S. Wang, J. Phys. Chem. B 108 (2004) 12259.
[168] H. Häkkinen, M. Moseler, O. Kostko, N. Morgner, M.A. Hoffmann, B. Issendorff, Phys. Rev. Lett. 93 (2004) 093401.
[169] J.M. Soler, I.L. Garzón, J.D. Joannopoulos, Solid State Commun. 117 (2001) 621.
[170] N.T. Wilson, R.L. Johnston, Eur. Phys. J. D 12 (2000) 161.
[171] S. Darby, T.V. Mortimer-Jones, R.L. Johnston, C. Roberts, J. Chem. Phys. 116 (2002) 1536.
[172] G. Rossi, A. Rapallo, C. Mottet, A. Fortunelli, F. Baletto, R. Ferrando, Phys. Rev. Lett. 93 (2004) 105503.
[173] M.P. Johansson, D. Sundholm, J. Vaara, Angew. Chem., Int. Ed. 43 (2004) 2678.
[174] Y. Kondo, K. Takayanagi, Science 289 (2000) 606.
[175] H. Tanaka, S. Neukemans, E. Janssens, R.E. Silverans, P. Lievens, J. Am. Chem. Soc. 125 (2003) 2862.
[176] S. Neukemans, E. Janssens, H. Tanaka, R.E. Silverans, P. Lievens, Phys. Rev. Lett. 90 (2003) 033401.
[177] E. Janssens, H. Tanaka, S. Neukemans, R.E. Silverans, P. Lievens, New J. Phys. 5 (2003) 46.
[178] X. Li, K. Boggaravarapu, J. Li, H.J. Zhai, L.-S. Wang, Angew. Chem., Int. Ed. 41 (2002) 4786.
[179] P. Pyykkö, N. Runeberg, Angew. Chem., Int. Ed. 41 (2002) 2174.
[180] J. Autschbach, B.A.J. Hess, M.P. Johansson, J. Neugebauer, P. Patzschke, P. Pyykkö, M. Reiner, D. Sundholm, Phys. Chem. Chem. Phys. 6 (2004) 11.
[181] H.-J. Zhai, J. Li, L.-S. Wang, J. Chem. Phys. 121 (2004) 8369.
[182] E.N. Esenturk, J. Fettinger, Y.-F. Lam, B. Eichhorn, Angew. Chem., Int. Ed. 43 (2004) 2132.
[183] S. Neukemans, E. Janssens, Z. Chen, P.v.R. Schleyer, P. Lievens, Phys. Rev. Lett. 92 (2004) 163401.
[184] X. Zhang, G. Li, X. Xing, X. Zhao, Z. Tang, Z. Gao, Rapid Commun. Mass Spectrom. 15 (2001) 2399.
[185] V. Kumar, Y. Kawazoe, Appl. Phys. Lett. 80 (2002) 859.
[186] Q. Kong, M. Chen, J. Dong, Z. Li, K. Fan, M. Zhou, J. Phys. Chem. A 106 (2002) 11709.

[187] H.-J. Himmel, A.J. Downs, J.C. Green, T.M. Greene, J. Phys. Chem. A 104 (2000) 3642.
[188] E. Janssens, S. Neukemans, F. Vanhoutte, R.E. Silverans, P. Lievens, A. Navaro-Vasquez, P.v.R. Schleyer, J. Chem. Phys. 118 (2003) 5862.
[189] A. Sekiguchi, Y. Ishida, Y. Kabe, M. Ichinohe, J. Am. Chem. Soc. 124 (2002) 8776.
[190] A. Schnepf, Angew. Chem., Int. Ed. 43 (2004) 664.
[191] A. Sekiguchi, M. Matsumo, M. Ichinohe, Science 275 (1997) 60.
[192] M. Ichinohe, N. Fukaya, A. Sekiguchi, Chem. Lett. (1998) 1045.
[193] A. Sekiguchi, N. Fukaya, M. Ichinohe, Y. Ishida, Eur. J. Inorg. Chem. (2000) 1155.
[194] S.-D. Li, H.-L. Yu, H.-S. Wu, Z.-H. Jin, J. Chem. Phys. 117 (2002) 9543.
[195] S.-D. Li, H.-L. Yu, H.-S. Wu, Z.-H. Jin, J. Chem. Phys. 119 (2003) 6750.
[196] R.B. King, Inorg. Chem. 42 (2003) 8755.
[197] A.C. Tsipis, C.A. Tsipis, J. Am. Chem. Soc. 125 (2003) 1136.
[198] A.C. Tsipis, E.E. Karagiannis, P.F. Kladou, C.A. Tsipis, J. Am. Chem. Soc. 126 (2004) 12916.
[199] S.-D. Li, G.-M. Ren, C.-Q. Miao, Z.-H. Jin, Angew. Chem., Int. Ed. 43 (2004) 1371.
[200] S.-D. Li, C.-Q. Miao, G.-M. Ren, Eur. J. Inorg. Chem. (2004) 2232.